

Elucidating Cellular Impacts of Hsp-independent CHIP Ubiquitination on Proteostasis

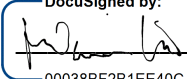
by
Emily June Connelly

DISSERTATION
Submitted in partial satisfaction of the requirements for degree of
DOCTOR OF PHILOSOPHY

in
Pharmaceutical Sciences and Pharmacogenomics

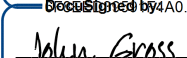
in the
GRADUATE DIVISION
of the
UNIVERSITY OF CALIFORNIA, SAN FRANCISCO

Approved:

DocuSigned by:

00038BF2B1EE40C... Melanie Ott
Chair

DocuSigned by:

4A0... Charles Craik

DocuSigned by:

72366174074B4F4... John Gross

Committee Members

Dedication

To my mom, who always wanted me to be a doctor. I know you wanted me to be an MD, but I think you would still be proud.

Acknowledgements

When I applied to UCSF, I opened Charly Craik's lab webpage and said that I would not want to join this lab, I don't want to work on proteases, the only thing less interesting is studying ubiquitination pathways. Charly's enthusiasm and the amazing work done by wonderful members of the Craik lab have convinced me that my first impression was wrong. To my advisor, Charly, thank you for having me in your lab and bringing together some of the most brilliant scientists I've had the pleasure collaborate and become friends with. I must thank all current and former members of the Craik lab (but especially Nick, Ing, Jamie, and Conner) for good times and great discussions. Thank you all for always being ready to commiserate or celebrate as appropriate. To my rotation mentor Beatrice, thanks for all the tasty baked goods, emotional support, and being a fantastic friend that's always willing to enable my various whims, from pottery to adopting additional cats. My thesis committee chair, Melanie Ott, and my committee member, John Gross, have provided me with immense amounts of advice and scientific input. I cannot thank either of you enough for the support you have provided.

To my family, Andrew, Donna and Steven, as well as our herds of cats (Stanley, Ollie, Baggie, Yvette, Winston, Simon and Morris), thank you for the daily support and distractions. Prajit, your advice and camaraderie from day 0 is greatly appreciated. I owe a huge thanks to Qi and Alex, my former managers at Assembly Biosciences. While I didn't quite hit the 4-year graduation goal Qi set for me, the mentorship you both gave and continue to give really helped me through the PhD. To my co-op supervisor at Regeneron, Giusy, and my colleagues (Darshi, Minhee, Iv, Baiye, and Larry), thanks for your patience, advice, and encouragement. I look forward to returning and working with you all more.

Finally, but likely most importantly, I have an enormous amount of gratitude for the members of the Craik lab CHIP bay. Dong hee, thank you for being a great mentor and friend. I'm grateful I was able to get the bench behind you so I could learn from you, and appreciate the zeal and rigor with which you approach scientific problems. Kristin and Shih-Wei, I am thankful for your friendships and all the instruction, help, and input. Thank you both for joining in on the CHIP project fun; the reason I say it's the best project is because of being able to work with you three in the CHIP bay.

Contributions

Chapter 1

The project described in Chapter 1 is in preparation for publication and has been an ongoing joint effort between me and Dr. Dong hee Chung. Dong hee provided significant experimental results and guidance throughout the project as well as training for biochemical methods and phage display. Dr. Kristin Wucherer and Dr. Shih-wei Chuo provided support for protein production, biochemical experiments, and structural studies, as well as insightful suggestions and training.

Chapter 2

This project is based on preliminary data generated by Dr. Matthew Ravalin (UCSF), Dr. Matthew Gardner and Professor Britt Glaunsinger (UC Berkeley). Dr. Shih-wei Chuo and Dr. Kristin Wucherer assisted with sample preparation for proteomics, and proteomics were performed by Creative Proteomics and MS Bioworks.

Chapter 3

This work was done in collaboration with Dr. Beatrice Ary (UCSF) and Dr. Andreas Puschnik (Chan Zuckerberg Biohub). Professor Melanie Ott provided valuable input and guidance.

Elucidating Cellular Impacts of Hsp-independent CHIP Ubiquitination on Proteostasis

By Emily June Connelly

Abstract

C-terminus of Heat-shock protein-70 interacting protein (CHIP) is an E3 ubiquitin ligase canonically known to mark misfolded Heat shock protein (Hsp) clients for degradation. A recent publication from the Craik lab demonstrated CHIP can directly interact with numerous proteins outside of Hsps. While the authors demonstrate the occurrence of Hsp-independent CHIP interactions in cells and that CHIP can ubiquitinate substrates without chaperones in biochemical assays, they were unable to show Hsp-independent substrate ubiquitination in cells. Successful demonstration of CHIP's Hsp-independent enzymatic activity in cellular contexts could elucidate molecular underpinnings of multiple disease states, including neurodegeneration, cancer, and viral infections, as well as provide insights into the feasibility using Hsp-independent CHIP interactions for targeted degradation of proteins.

Towards this goal, we developed CHIP inhibitors and further characterized a predicted Hsp-independent CHIP interaction with a human herpes virus 8 (HHV-8) protein. Previous approaches used peptides to competitively inhibit CHIP substrate binding, so we instead generated recombinant antibodies to inhibit CHIP's functions. These were shown to have distinct epitopes and were able to inhibit both CHIP substrate binding and ubiquitination. When reformatted into scFvs for intracellular expression, these antibodies can bind to CHIP and maintain some level of inhibitory function. The recombinant antibodies can be used to examine molecular mechanisms of CHIP interactions in disease states and enable structural studies. Next, we examined the predicted, Hsp-independent, CHIP interaction with the HHV-8 protein ORF28. Data indicates this interaction occurs in cells, and preliminary results show this interaction may be a mechanism of host protein regulation. Further studies will allow for non-biased identification of interactors and determination of the impacts of these interactions on viral replication.

Table of Contents

Chapter 1 : Conformationally Selective Recombinant Antibodies Inhibit Enzymatic

Activity of the E3 Ubiquitin Ligase CHIP via Multiple Mechanisms	1
1.1 Abstract	2
1.2 Introduction	2
1.3 Results.....	6
1.4 Discussion	13
1.5 Materials and Methods	14
1.6 Figures and Tables	24
1.7 References	30

Chapter 2: HHV-8's ORF28 interacts with host-protein CHIP to mediate

ubiquitination of host proteins.....	35
2.1 Abstract	36
2.2 Introduction	36
2.3 Results.....	39
2.4 Discussion	44
2.5 Materials and Methods	46
2.7 References	59

Chapter 3 : Generation of a SARS-CoV-2 RNA Replicon for Antiviral Drug Screening	64
3.1 Abstract	65
3.2 Introduction	65
3.3 Results	67
3.4 Discussion	69
3.5 Materials and Methods	65
3.6 Figures	75
3.7 References	79
Concluding remarks	82

List of Figures

Figure 1.1: Biological panning identified multiple recombinant antibodies against CHIP	24
Figure 1.2: High affinity Fabs with varying epitopes were identified from round 3	25
Figure 1.3: Negative stain and mass photometry provide insights into Fab binding modalities and epitopes	26
Figure 1.4: CHIP Fabs can inhibit CHIP E3 function and CHIP binding activity	27
Figure 1.5: scFv versions of the recombinant antibodies against CHIP are able to bind and inhibit cellular CHIP when overexpressed in cells	28
Supplementary Figure 1.1: Additional mass photometry.	29
Figure 2.1: The C-terminus of ORF28 has a high affinity for CHIP	51
Figure 2.2: CHIP associates with HAORF28, but not HA-ORF28 Δ C-term, in HEK293Ts	52
Figure 2.3: CHIP+ORF28 interaction reduces ORF28 stability and induces ubiquitination of nearby host proteins on the cell membrane.	53
Figure 2.4: IP-MS hits enrich for mRNA processing pathways	54
Figure 2.5: Ubiquitin remnant profiling shows increased ubiquitination of catabolism and proteasome related proteins.	55
Figure 3.1: Overview of SARS-CoV-2 replicons tested	75
Figure 3.2: Transfected Vero cells show evidence of RNA replication	76
Figure 3.3: Reporter levels in SARS-CoV-2 replicon bearing cells show minimal response to known replication inhibitors.	77
Supplementary Figure 3.1: Alternative replicon designs tested	78

List of Tables

Table 1.1: Kd determined by BLI of each Fab to CHIP or CHIP domains with Fab on the tip ...	29
Table 2.1: IP-MS hits from HAORF28 in HEK293T cells	55
Table 2.2: Upregulated ubiquitination sites in HEK293T cells expressing HAORF28	57
Table 2.3: Downregulated ubiquitination sites in HEK293T cells expressing HAORF28	58

**Chapter 1: Conformationally Selective Recombinant Antibodies Inhibit
Enzymatic Activity of the E3 Ubiquitin Ligase CHIP via Multiple
Mechanisms**

1.1 Abstract

Carboxyl-terminus of Hsp70-Interacting Protein (CHIP) is an E3 ubiquitin ligase canonically known to mark misfolded chaperone clients for degradation. Recent publications, including work from the Craik lab, indicate CHIP has a previously underappreciated role in chaperone-independent substrate ubiquitination.¹ Dysregulation of CHIP has been implicated across multiple disease states, including cystic fibrosis, neurodegeneration, and cancer, suggesting CHIP may be a therapeutically relevant target in multiple indications. However, the full extent of CHIP's impact on the proteome remains uncharacterized, partially due to a dearth of specific and potent inhibitors. To address this, the novel phage display method Rare Antibody Phage Isolation and Discriminatory screen (RAPID) was applied to CHIP to identify twelve conformationally-selective, recombinant antibodies against CHIP. The affinity of these recombinant antibodies against full-length and subdomains of CHIP were assayed and ranked. Six of the higher affinity Fabs were further characterized to determine their inhibition of three CHIP functions: CHIP-TPR substrate binding, auto-ubiquitination, and substrate ubiquitination. Despite maintaining distinct epitopes, five Fabs demonstrate inhibition of varying combinations of CHIP functions in biochemical assays and show translatability into cellular systems.

1.2 Introduction

The ubiquitin-proteasome system (UPS) is a crucial cellular pathway responsible for the degradation of damaged, misfolded, or excessive proteins in the cell. The UPS is composed of ubiquitin, E1, E2, and E3 enzymes, and the proteasome. The E3's are the most diverse set of the UPS proteins, and determine the targets of the ubiquitination reaction.² Ubiquitin molecules are covalently linked to the target protein by the E1 (ubiquitin activator), E2 (ubiquitin conjugator)

and E3 (ubiquitin ligase). The process is repeated until a ubiquitin chain is formed, after which the protein is recognized by the proteasome and degraded.

CHIP (carboxyl terminus of Hsc70-interacting protein) is an E3 ubiquitin ligase that plays a crucial role in the regulation of proteostasis. The protein is composed of three domains: an N-terminal tetratricopeptide repeat (TPR) domain, a charged coiled-coil (CC) domain, and a C-terminal U-box domain. CHIP's coil-coil region induces dimerization, and it was thought homodimeric assembly was required for function as an E3 ubiquitin ligase. The TPR domain of CHIP is canonically known to bind to the C-termini of the cellular chaperones heat shock protein (Hsp) 70 and 90. The interaction between the chaperone C-terminus and CHIP mediates the transfer of ubiquitin from the E2 bound at CHIP's U-box to the Hsp client.³ Through this process CHIP is canonically known to mediate ubiquitination of Hsp 70/90 clients to prevent the accumulation of misfolded proteins during proteostasis.⁴ In addition to assisting in clearance of misfolded clients, CHIP regulates levels of Hsp70 and other Hsp chaperones. CHIP ubiquitinates Hsp70 and targets it for proteasomal degradation, resolving cellular stress response.⁵

While these classical functions of CHIP are well described, recent work suggests CHIP may perform additional role in proteostasis. The paradigm of CHIP function being chaperone-dependent is challenged by data indicating the specificity of CHIP binding compasses C-termini beyond Hsps. Many of these C-termini are formed through proteolytic cleavage by capsases, including caspase-6. These interactions suggest CHIP may mediate ubiquitination in undescribed C-degron pathway occurring in parallel to CHIP's canonical, Hsp-dependent pathway. Based on empirical binding data, 2700 new, Hsp-independent CHIP interactors were predicted beyond caspase-6, suggesting this pathway may impact a variety of diseases states. CHIP can bind to and inhibit the active form of caspase-6, indicating the production of Hsp-independent CHIP

interactors may be at least partially self-regulating. This also suggests CHIP may be able to regulate apoptosis by inhibiting caspase-6.¹ Separately, CHIP's function was presumed to be dependent on homodimerization. However, it seems while the dimeric version of CHIP favors the ubiquitination of Hsp clients, the monomeric version of CHIP favors Hsp-independent ubiquitination, and the dimer/monomer conformation is dependent on CHIP autoubiquitination.⁶

CHIP is seeing a resurgence of interest due to its role in multiple disease states and potential as a proteolysis-targeting chimera (PROTAC). Recent publications have identified CHIP as a regulator of IFN γ response in tumor cells, and that knockdown or knockout of CHIP sensitizes tumors to anti-PD1 therapy.^{7,8} By interacting with CHIC2, a transmembrane protein, CHIP regulates levels of CSF2RB, a common component of IL-3, IL-5, and GM-CSF receptors.⁹ CHIP also plays a more well described role in cystic fibrosis by regulating CFTR levels, as well as in neurodegeneration by modulating tau and huntingtin levels.^{10,11} In addition, with CHIP's ability to ubiquitinate targets in a chaperone independent manner, its utility as a PROTAC effector is now much greater.¹² However, CHIP's multi-faceted function means its precise role in these disease states and potential as a PROTAC effector require additional studies.

Given the new chaperone-independent role CHIP may play in proteostasis in addition to its canonical function, there is a need for novel inhibitors of CHIP functions. Currently described CHIP inhibitors are peptides or small molecules. Two peptide-based CHIP inhibitors have high affinity for CHIP's TPR domain, and prevent CHIP from binding to native substrates. However, both the linear CHIP-Opt peptide and the cyclic peptide are competitive inhibitors with poor cell membrane permeability.^{13,14} Small molecule inhibitors have also been identified. One inhibitor was able to inhibit ubiquitination in the high-micromolar range, but TPR binding inhibition was not examined and a potential mechanism of action was not identified.¹⁵ Another small molecule

inhibitor of CHIP was identified using differential scanning fluorimetry, and was capable of inhibiting both substrate binding and ubiquitination in the high-micromolar range. Intriguingly, this inhibition seems to be caused by allosteric modification after the small molecule binds to the coil-coil region of a CHIP dimer.¹⁶ These inhibitors provide basis for developing more potent inhibitors, but additional inhibitors with better potency, targeting, and additional mechanisms of action need to be developed.

Recombinant antibodies can function as inhibitors and are able to target sections of proteins that are generally inaccessible to small molecules. Phage display, hybridoma, and yeast display systems allow for the isolation of antibodies that can bind to specific intracellular targets. By overexpressing these recombinant antibodies in cells, a specific protein can be targeted, and then activity or other protein-protein interactions can be inhibited. This allows for the examination of the roles the protein and its interactions have on cellular processes.¹⁷⁻¹⁹ This approach could allow for the development of inhibitors against E2 recruitment to the CHIP U-Box or impact the dimer/monomer equilibrium, in addition to potentially functioning as inhibitors of TPR binding like many of the described inhibitors.

Previously, we have successfully reformatted recombinant fragments antigen-binding (Fabs) isolated from a naïve B-cell phage display library into single-chain variable fragments (scFvs), and disrupted protein-protein interactions in cells by overexpressing the scFvs intracellularly.²⁰ To generate a novel set of CHIP inhibitors, we applied a newly developed phage display method to identify recombinant antibodies against CHIP, which is a challenging biopanning target due to its homodimeric structure and conformational flexibility. Twelve unique Fabs were identified, and inhibitory activity against CHIP TPR binding and its E3 function by these Fabs were tested biochemically. Studies were focused on six Fabs with affinity for CHIP and inhibitory function

in biochemical assays, and these Fabs were reformatted into scFvs for cellular studies. These scFvs can bind to CHIP and disrupt some CHIP function in cells. These antibodies represent a novel class of inhibitors and are likely inhibiting CHIP function via multiple mechanisms.

1.3 Results

Biological panning of Fabs against CHIP

Four rounds of biopanning were performed against CHIP using previously described methods.²¹ Briefly, our recombinant phage library was incubated with biotinylated CHIP conjugated to magnetic beads, and low-affinity binders were removed by washes of increasing stringency. Anti-Myc selections were performed after round 2 to reduce enrichment of Myc-tag binding phage (**Figure 1.1a**). Individual colonies were picked, and periplasmic extracts (PPE) generated to assay for production of Myc-tagged Fab via dot blot. While there were multiple positive hits on the dot blots, indicating production of full-length Fab, the majority of these Fabs had low affinity (high μM Kd) to CHIP. This is likely related to the fact CHIP is a challenging biopanning target due to its homodimeric structure and conformational flexibility.

To identify high-affinity binders from the campaign, the recently described Phage Isolation and Discriminatory screen (RAPID) method was used. Outputs from each round of panning were fluorescently labelled and assessed via flow cytometry to identify the most promising round to screen for high-affinity binders. When enrichment for antigen binding phage occurs, the fluorescence peak shifts right (**Figure 1.1b**). Round 3 had the most enrichment with normalized mean fluorescence intensity of 2.11, suggesting a hit rate of 10-50% (**Figure 1.1c**). PPE from round 3 colonies were used in dot blots and Biolayer interferometry antibody screen (BIAS) to screen for CHIP binders. The dot blots indicated 80% of wells contained Fabs with Myc-tags (**Figure 1.1d**). Meanwhile, BIAS only flagged 19% of wells as having Fabs that can

bind to CHIP, in line with the predicted hit rate from the flow analysis (**Figure 1.1e**). BIAS was used to screen 190 clones, and all positives were sequenced. This yielded twelve unique Fabs. Each of these Fabs were overexpressed and their Kd against CHIP was determined via BLI with CHIP on the tip. These Fabs had preliminary Kds ranging between 5-300nM for CHIP (data not shown). While these Kds were superseded by better BLI methodology, these data were used to select six high-affinity (10-200 nM) Fabs for further characterization of both binding and functional inhibitory activity.

Selected Fabs have distinct epitopes on CHIP

BLI was performed against full length CHIP, the TPR, and CHIP Ubox/CC for epitope binning. Each Fab was biotinylated and loaded onto the tip, and then CHIP associated to the Fabs in the association step. These results suggest the Fabs fall in at least three distinct categories. First, D6 and H2 have reasonable affinity for CHIP full length with Kds at 140 and 210 nM respectively (**Figure 1.2a** and **Table 1.1**). However, neither Fab has affinity for the Ubox/CC (**Figure 1.2b**), but both have affinity for the TPR (**Figure 1.2c**). Next, 2C5 binds to CHIP with moderate affinity (Kd 140 nM), but has a similar affinity to both Ubox/CC and TPR (**Figure 1.2a, b, and c**). Finally, Fabs 2D11, 2F1, and 2G7 have the highest affinity for CHIP out of the examined Fabs with Kds for full length CHIP in the 25-55 nM range (**Figure 1.2a** and **Table 1.1**). These Fabs do not bind to TPR (**Figure 1.2c**), but do bind to the Ubox/CC (**Figure 1.2b**).

After examining the binding of these Fabs to CHIP and CHIP domains, overlap in epitopes between the Fabs was assessed using competitive BLI. Similar in principle to competitive ELISA, this assay allows for the examination of if a Fab occludes or competes for an epitope with a second Fab. Based on this, D6 does not pair well with D6, H2, or 2C5, regardless of order, but is capable of middling co-association with 2D11, 2F1, and 2G7. Fab H2 is unable to bind to

the same CHIP dimer as any other Fab, including a second H2, regardless of if H2 is loaded first or second. Associating 2C5 and 2G7 first reduces the ability of a second Fab to associate to the same CHIP dimer, but both are able to associate with CHIP as the second Fab. When 2D11 associates first, both 2F1 and 2G7 are successful in associating with the same CHIP dimer, suggesting 2D11 does not have an overlapping epitope with either Fab, and that the conformation of CHIP it binds to is compatible for 2F1 and 2G7 binding (**Figure 1.2d**).

CHIP with 2F1 bound can have every Fab, except H2 and 2G7, for the second Fab association. This is the only Fab able to have a second Fab of the same kind bind in the second association, suggesting 2F1 is a true 2 Fab:1 CHIP dimer binder. When increasing the concentration of 2F1 in the first association to be 2x the original experiments, the second association into 2F1 shows no binding, indicating all binding spots are saturated with the increased concentration of 2F1. However, 2D11, 2C5 and D6 are all able to bind to CHIP with the 2x 2F1 CHIP association 1, suggesting these epitopes are distinct from 2F1. Meanwhile, 2G7 shows reduced binding in the 2x 2F1 association 1 condition, suggesting the epitopes between 2F1 and 2G7 have some overlap (**Figure 1.2d**).

To further examine presumed epitopes and binding modalities, negative stain and mass photometry were performed. For D6, the micrographs indicate the Fab mostly binds to the TPR domain on one side of CHIP (**Figure 1.3a**). This matches with the BLI data, as well as the mass photometry, which shows a mass shift corresponding to the molecular weight of one CHIP dimer with one Fab (**Figure 1.3b**). In the case of 2D11, the negative stain suggests that the binding site is closer to the Ubox of CHIP (**Figure 1.3c**). Only one Fab is observed binding to a CHIP dimer in the micrograph, corroborating the mass photometry data where the second peak is the size of a CHIP dimer with one monomer (**Figure 1.3d**). The Fab 2F1 was the only Fab capable of binding

in a 2:1 manner via mass photometry, and this appears to be replicated in the negative stain, where two Fabs can be seen binding to CHIP close to the TPR-Ubox interface (**Figure 1.3e**). The second peak in the mass photometry shifts further right for 2F1 compared to the other examined Fabs, and the molecular weight corresponds to that of 2 Fabs bound to 1 CHIP dimer (**Figure 1.3f**). While 2G7's micrographs are not able to provide conclusive insights into its epitope, it does not bind to the TPR (**Figure 1.3g**). Intriguingly, in addition to the typical 1 Fab+1 CHIP dimer peak on the mass photometry, 2G7 also has an intermediate peak at the size corresponding to approximately 1 CHIP monomer and 1 Fab (**Figure 1.3h**).

Recombinant antibodies can inhibit CHIP function in vitro and in cells

Inhibition of CHIP function by these Fabs were examined both *in vitro* and in cells. Substrate and auto ubiquitination inhibition was screened at a final fab concentration of 5 μ M to determine which Fabs inhibit each function (**Figure 1.4a**). From these assays, it was determined three Fabs inhibit autoubiquitination, and one increases it (**Figure 1.4b**). All Fabs except 2C5 decrease substrate (Hsp70) ubiquitination *in vitro* (**Figure 1.4c**). TPR binding inhibition was examined by fluorescence polarization, and three Fabs had an IC₅₀ below 5 μ M (**Figure 1.4g**).

Next, the Fabs were reformatted into scFvs for cellular studies, as these generally fold better than Fabs in the reducing environment of the mammalian cytosol. To assess if the recombinant antibodies maintain their affinity for CHIP after the reformat from Fab to scFv, immunoprecipitation was done against the tagged scFvs to determine if CHIP co-immunoprecipitated after intracellular scFv expression (**Figure 1.5a**). Next, we examined if the scFvs could inhibit CHIP substrate binding in cells using a previously described Nano-bit system.¹³ Here, only one scFv successfully inhibited CHIP TPR binding in cells (**Figure 1.5b**). Finally, with CHIP's newly described role in regulating IFNGR1 stability, the ability of these

scFvs to stabilize the receptor by inhibiting CHIP E3 function and increase interferon-stimulated response element (ISRE) transcription was examined in melanoma cells. Here, two scFvs were able to increase transcription of CD274 (PDL-1), an ISRE of significant interest due to the rise of immune checkpoint inhibitors (**Figure 1.5c**). Individual antibody's inhibitory functions are described below to better put the inhibition in the context of presumed epitope.

D6 reduces CHIP substrate binding, but is only a moderate inhibitor of substrate ubiquitination

The epitope of D6 is likely on the TPR based on the epitope binning, which would suggest it could function as a CHIP substrate binding inhibitor, and thus reduce ubiquitination. This would be aligned with the described peptide-based competitive inhibitors of CHIP. D6 was able to inhibit CHIP substrate binding in fluorescence polarization assay, with an IC₅₀ of around 2 uM (**Figure 1.4g**). After reformatting to an scFv, overexpressed D6 can pull down endogenous CHIP (**Figure 1.5a**). Furthermore, inhibition of substrate binding by overexpressed D6 occurs in the nano-BIT complementation cells (**Figure 1.5b**). However, D6 is only a middling inhibitor of CHIP substrate inhibition *in vitro* (**Figure 1.4a**). Notably, D6 is the only Fab demonstrating increase in autoubiquitination *in vitro* (**Figure 1.4b**). Subsequent experiments demonstrated it is unable to regulate ubiquitination in cells, a surprising result given the inability CHIP to bind to substrates to mediate ubiquitination.

H2 reduces CHIP substrate binding in vitro, but does not function in cells

Like D6, H2 has affinity for CHIP and CHIP TPR, and can inhibit substrate binding *in vitro* with an IC₅₀ of 1 uM (**Figure 1.4g**). While the H2 scFv can fold and co-immunoprecipitate CHIP with it, H2 is unable to impact substrate binding in cells (**Figure 1.5a and b**). H2 inhibits substrate ubiquitination *in vitro*, but in contrast to D6, it does not impact autoubiquitination (**Figure 1.4b and c**). Despite seemingly overlapping epitopes between H2 and D6 based on the

BLI results, D6 and H2 function distinctly. While H2 can inhibit substrate binding and substrate ubiquitination *in vitro*, D6 can do these inhibitory functions while also inhibiting substrate binding in cells and increasing autoubiquitination *in vitro*. This suggests that while the epitopes are close to each other, the exact contacts are likely distinct.

2C5 does not significantly inhibit CHIP function

While 2C5 binds to CHIP, Ubox/CC and TPR, 2C5 does not significantly inhibit CHIP function. Fab 2C5 does fold as an scFv after reformatting and co-immunoprecipitated CHIP to a greater degree than most of the other scFvs (**Figure 1.5a**). However, despite its affinity for CHIP TPR, it does not inhibit CHIP substrate binding via fluorescent polarization (**Figure 1.4g**) or in cells (**Figure 1.5b**). Additionally, it does not significantly inhibit substrate or auto-ubiquitination *in vitro*, except for a slight reduction in substrate ubiquitination at 10 uM (**Figure 1.4e and f**). This indicates the epitope is neither occluding an auto-ubiquitination site nor E2 recruitment. Combined with the BLI data, it is suspected the epitope recognized by 2C5 has little to no conformational flexibility and is in a highly conserved region in the asymmetric homodimer.

2D11 inhibits both substrate and autoubiquitination

2D11 has one of the highest affinities for CHIP among the featured antibodies and can reduce ubiquitination without binding to CHIP TPR or impacting substrate binding. This antibody is unable to significantly inhibit CHIP substrate binding in either biochemical or cellular contexts (**Figure 1.4g** and **Figure 1.5b**). However, 2D11 is a powerful inhibitor of both autoubiquitination and substrate ubiquitination *in vitro* (**Figure 1.4g**). While 2D11 associates with endogenous CHIP in cells, it is unable to regulate ISRE (**Figure 1.5b and c**). Despite not showing immediate utility in cells, this Fab represents the first inhibitor described in this study with a novel mechanism of inhibition of CHIP function. Based on the previously described

epitope binning studies, it appears 2D11 prevents ubiquitination by inhibiting recruitment ubiquitination machinery to the UBox instead of inhibiting CHIP substrate binding, and is binding somewhere on the dimer interface given the 1Fab:1CHIP dimer binding ratio.

2F1 inhibits substrate binding in vitro but not in cells, and is the best ubiquitination inhibitor

2F1 is the other highest affinity CHIP antibody described in this work. This antibody can reduce substrate binding in vitro with an IC₅₀ of 2.5 uM, despite having no affinity to the CHIP TPR (**Figure 1.4g**). After the reformat to scFv, 2F1 appears to keep a high affinity for CHIP as it co-immunoprecipitated the most CHIP out of the examined antibodies (**Figure 1.5a**). This maintained affinity for CHIP did not translate to maintaining its ability to inhibit substrate binding in cells (**Figure 1.5b**). Meanwhile, 2F1 is the best inhibitor of both autoubiquitination and substrate ubiquitination *in vitro* (**Figure 1.4e and f**). This function translates to cells, where SK-MEL-28 cells overexpressing 2F1 demonstrate an increase in ISRE transcription, suggesting the scFv is inhibiting CHIP's ubiquitination of IFNGR1 (**Figure 1.5c**). Negative stain indicates 2F1 binds to near the UBOX, without directly binding to the E2 recruitment site. Furthermore, the BLI, negative stain, and mass photometry all indicate 2F1 binds to CHIP in a 2 Fab:1 CHIP dimer manner. This represents a distinct mechanism of regulation of CHIP function from 2D11, as 2F1 has two binding sites per CHIP dimer. 2F1 may prevent ubiquitination by inhibiting recruitment ubiquitination machinery and inhibits each monomer of the CHIP dimer.

2G7 has a potentially overlapping epitope with 2F1, but it does not inhibit substrate binding

While 2G7 and 2F1 may have some overlap in epitopes based on the competitive BLI, they are functionally distinct. Unlike 2F1, 2G7 has no ability to inhibit substrate binding *in vitro* (**Figure 1.4g**). For ubiquitination, 2G7 is a strong inhibitor of both substrate ubiquitination and CHIP autoubiquitination (**Figure 1.4e and f**). This inhibition carries over to cells, as 2G7 is the

only scFv besides 2F1 that can increase ISRE transcription (**Figure 1.5c**). The overlap in epitopes between 2F1 and 2G7 based on the competitive BLI and overlap in functional inhibition in cells suggest these antibodies could be binding near each other, but the epitope for 2F1 allows for 2 Fab to 1 dimer binding, while the 2G7 epitope does not.

1.4 Discussion

We have successfully identified six recombinant antibodies with varied epitopes against CHIP that demonstrate unique combinations of CHIP inhibition. While D6 and H2 both inhibit substrate binding, both are comparatively poor substrate ubiquitination inhibitors. D6 is also the only antibody that demonstrates an increase in CHIP autoubiquitination *in vitro*. With autoubiquitination reported to regulate the equilibrium between monomeric and dimeric CHIP, future cellular studies involving D6 could examine if overexpression of D6 alters the dimer-monomer equilibrium in cells. While 2C5 is unable to inhibit CHIP function, its affinity for CHIP could allow for it to be used as part of a PROTAC by allowing for recruitment of a protein to CHIP. 2D11, 2F1 and 2G7 are strong inhibitors of ubiquitination, and all have slightly different epitopes. These represent a novel class of CHIP ubiquitination inhibitors, as they are likely preventing the recruitment of E2s to the CHIP Ubox.

These recombinant antibodies against CHIP can enable elucidation of how specific CHIP activities like substrate binding, ubiquitination, autoubiquitination, and the dimer/monomer equilibrium impact CHIP's role in proteostasis. By combining these antibodies with new adeno-associated virus (AAV) vectors and other methods of targeted gene therapy delivery, researchers can gain additional temporal control of when inhibition starts, as well as targeting specific cell types of interest.^{22,23} This is especially important for broadly expressed proteins like CHIP, as the function in one disease state or cell type may be distinct from another. For example, inhibition of

CHIP in tumors may be favorable due to CHIP's role in regulating IFN γ signaling, but inhibition may be unfavorable in the immune cells responsible for clearing the tumor cells.

1.5 Materials and Methods

Protein purification

All proteins were produced in BL21(DE3) *Escherichia coli*.

CHIP expression and purification

CHIP and various CHIP mutant constructs were expressed from pET151 constructs. All versions N-terminally code for a tobacco etch virus- (TEV)-cleavable His-Tag. *E. coli* were grown in terrific broth at 37 °C until induction with 500 μ M IPTG during log growth phase. Cultures were cooled to 18 °C and incubated overnight. Cultures were collected by centrifugation and resuspended in binding buffer (50mM Tris pH8.0, 10mM imidazole and 500mM NaCl) supplemented with protease-inhibitor. Resuspended cells were then sonicated and clarified. Supernatant was incubated with Ni-NTA His-Bind Resin, which was then washed with binding buffer and His wash buffer (50mM Tris pH8.0, 30mM imidazole and 300mM NaCl). Protein was eluted from the beads with His elution buffer (50mM Tris pH8.0, 300mM imidazole and 300mM NaCl). To remove the His tag, protein was incubated overnight with TEV protease at 4°C. Sample was run through His-Bind resin to remove uncleaved product, cleaved His-tags, and TEV from the solution. Sample was then run through size exclusion chromatography (SEC) (Hiload 16/600 superdex 200) in 50mM HEPES pH7.4, 150mM NaCl for final purification.

Fab expression and purification

Fabs were expressed using previously described methods.²⁴ The pelB signaling peptide was used for secretion into periplasm for proper folding of Fabs and C-terminally His(6x) tags and Myc tags were designed for downstream purification and IP studies. Starter cultures of BL21(DE3)

containing phagemid were grown overnight at 30°C in 2xYT, 2% glucose, 100ug/mL ampicillin. Cultures were diluted into fresh 2xYT, 0.1% glucose, 100ug/mL ampicillin and cultured at 37°C until OD600 reached ~0.6. Cells were induced with 1 mM final concentration of IPTG and incubated overnight at 20°C. Cells were lysed using osmotic shock for periplasmic extraction. Overnight cultures were collected by centrifugation and 15 mL of ice-cold TES buffer (200 mM Tris pH 8.0, 0.5 mM EDTA, 0.5 M Sucrose) per 1L culture was added and incubated for 60 minutes at 4°C with gentle shaking. Ice cold water was added to a total solution volume of 50 mL, and the solution was incubated for an additional 45 minutes. The soluble fraction of the lysis was collected by centrifugation (10,000 g for 15 min). 100 µL of 1M MgCl₂ and imidazole to a final concentration of 10 mM was added to each set of supernatant. Samples were batch bound with Ni-NTA His-Bind Resin for at least one hour at 4°C. Beads were washed with Fab wash buffer 1 (50 mM Tris pH 8, 250 mM NaCl, filtered) and Fab wash buffer 2 (50 mM Tris pH 8, 500 mM NaCl, 20 mM Imidazole). Fabs were eluted using Fab elution buffer (50 mM Tris pH 8, 500 mM NaCl, 500 mM Imidazole) and then dialyzed against CHIP Fab buffer (50 mM HEPES and 150 mM KCl, pH 7.4) overnight. SEC (Superdex 200) was performed for final purification.

Phage display

Standard biopanning with magnetic beads was performed as previously described^{24,25}. CHIP was chemically biotinylated using the EZ-link biotinylation kit (Pierce, #21425) and immobilized to Dynabeads streptavidin beads (Invitrogen, #65305) in CHIP buffer (50mM HEPES pH7.4, 25 mM KCl, 1mM TCEP). A human naïve B-cell phage-displayed Fab library (diversity 4.1 x10¹⁰) in CHIP phage buffer (50 mM HEPES pH 7.4, 25 mM KCl) was introduced to the antigen-beads. Low-affinity binders were removed with washes of increasing amounts each round of phage buffer and wash buffer (50mM HEPES pH7.4, 25 mM KCl, .1% Tween-20). Negative selections against

magnetic beads with N-terminally biotinylated Myc peptides started at round 2 to reduce enrichment of Myc binding phage. Output phage were infected into TG-1 *E. coli* and the sub library reamplified for the next round of panning.

Phage amplification

Fab-displayed phage were amplified and prepared using standard methods. Briefly, 50 ml cultures (2xYT, 2% glucose, 100 ug/ml Ampicillin) of phagemid-infected TG-1 *E. coli* cells were incubated at 37°C at 200 rpm shaking until an OD600 of ~0.5. Next, 10 ml of this culture was infected with M13KO7 helper phage to cell ratio of 10:1. The culture was then incubated at 37°C for 30 min without shaking followed by a 20 min 37°C incubation with shaking at 200 rpm. Infected cells were collected by centrifugation and resuspended in fresh media (2xYT 100 mg/ml Ampicillin, 50 mg/ml Kanamycin). Cultures were grown overnight, and amplified phage were isolated by adding .2x volume PEG 6000/2.5M NaCl phage to the supernatant of the overnight cultures. Phage yields were analyzed by OD268 measurements.

Periplasmic extraction (PPE)

Individual clones were inoculated into 2xYT media containing 2% glucose and 100 mg/ml ampicillin in round bottom 96 well plates (150 ul of media per well). Cultures were grown overnight at 37°C with 200 rpm shaking. The next day, 12 ul of overnight culture was inoculated into 96 well deep plates containing 2xYT media with 0.1% glucose and 100 mg/ml Ampicillin (1200ul of media per well) and grown for 4-6 hours until culture was turbid. Fab expression was induced with 300 ul of 2xYT, 100 mg/ml ampicillin and 5 mM IPTG. Cultures were incubated overnight at 30°C with 200 rpm shaking. Periplasmic extracts were collected by osmotic shock. Briefly, cells from the induced overnight cultures were collected by centrifugation at 2000 g for 25 min and the supernatant removed. Next, 375 ul of ice-cold TES buffer (200 mM Tris-HCl, 500

mM EDTA, 500 mM sucrose, pH 8) was added directly into each well and incubated with shaking at RT to resuspend the pellet. Subsequently, 1125 ul of ice-cold water was added to each well and mixed thoroughly. The prep was centrifuged at 2000 g for 25 min, and the periplasmic extract (supernatant) was stored at -20 °C for future experiments.

Dot blots

From 96-well periplasmic extracts, 2-3 ul from each well were applied to nitrocellulose membranes. After allowing the samples to absorb for ~10 min, the membrane was blocked with 2% milk in TBS and gently rocked at RT for one hour. The membrane was washed with TBS-T (0.05% Tween-20) thrice and then incubated with anti-Myc HRP(9E10) antibody (1:5000 dilution) in 1% milk in TBS for 1 hr. Membranes were washed with TBS-T (x2) and TBS (x2), then imaged.

Bio-layer interferometry (BLI)

All buffers were filter sterilized with 0.22 mm filters prior to preparing samples. Kinetic constants of the Fabs were determined by Octet RED384 system. BLI plates were set up in black 384 well microplates and streptavidin tips (Sartorius, 18-5019) were used to load the biotinylated antigen (CHIP, CHIP domains, Fab). Data were analyzed using 1:1 interaction model on the ForteBio data analysis software 12.0.

Phage labeling with NHS-FITC

NHS-Fluorescein (Thermo Scientific) was prepared in DMSO (1 mg/ml final concentration). For one hour at room temperature, 50 ul of NHS-FITC (1mg/ml) 500 ul of phage in CHIP phage buffer ($OD_{268} = 1$, final), and 40 ul of .67 M Borate buffer were incubated together in the dark. A .2 volume of PEG 6000/2.5M NaCl was added to the reaction to precipitate phage and incubated on ice for 15 min. Precipitated phage were collected by centrifugation (max speed for 5 min) and supernatant was removed. Pellets were resuspended in CHIP phage buffer and the process was

repeated twice more to remove free NHS-Fluorescein. Samples were immediately used in subsequent flow cytometry experiments.

Flow cytometry

Biotinylated CHIP was immobilized onto SPHERO™ Streptavidin Polystyrene particles, (3.0 – 3.9 µm). Prior to adding antigen, the beads were blocked with 2% BSA- buffer for 1 hour. Beads were then washed three times by resuspending beads in 1% BSA-buffer and subsequently centrifuging the beads (7k rpm for 2 min). Biotinylated CHIP was then added to beads at 1% BSA CHIP buffer final concentration and incubated for one hour. Meanwhile, labeled phage from each round of panning were blocked in 1% BSA CHIP phage buffer for one hour. After the beads were washed, blocked phage were added to the beads and incubated for 1-1.5 hours. After the binding phase, beads were washed 1-3 times with 1%BSA-CHIP phage buffer and passed through a 40 µm cell strainer. Flow cytometry analysis were performed on a benchtop Beckman Cytoflex Analyzer or BDFACSCaliber machine. Bead populations were gated with FSC and SSC parameters and only singlet populations were analyzed by gating linear FSA and FSW. Of singlet population of beads, histogram analysis was done with FITC.

Biolayer interferometry antibody screen (BIAS)

Instrument and reagent set up was identical to that of standard BLI. Anti-myc Ab (9E10) (Sigma) was spiked into the Assoc-2. BLI was run in the following method: Assoc-1 (3 min), Assoc-2 (2 min 30 sec), and Dissoc (3 min). Raw data files of the run(s) were then used in the BATCH program to rank order candidate hits according to their predicted dissociation rates.

Mass photometry (MP)

The MP experiments were carried out on a OneMP mass photometer (Refeyn Ltd, Oxford, UK) at room temperature. Microscope coverslips (24 × 50 mm, Fisher Scientific, and 24 × 24 mm,

Globe Scientific) were cleaned by at least 3 cycles of rinsing with isopropanol and H₂O, followed by drying them under a stream of nitrogen. Clean coverslips were assembled using CultureWell™ reusable silicon gaskets (Grace Bio-Labs, # 103250). CHIP was incubated with the CHIP Fab at a 1:2 molar ratio at 4°C overnight. Before each measurement, the CHIP or CHIP-Fab sample was diluted immediately in 20 µL of MP buffer (50 mM HEPES, 50 mM KCl, pH 7.4) to reach final concentration of 50 nM of CHIP or CHIP-Fab, followed by data acquisition for 100 s at a 1 kHz frame rate using AcquireMP software (Refeyn Ltd.), and data analysis was carried out using DiscoverMP software (Refeyn Ltd.).

Electron microscopy-negative stain

Recombinant CHIP and Fab were prepared as above description. Specimens were prepared using the conventional negative staining procedure. Briefly, CHIP was incubated with the CHIP Fab at a 1:2 or 1:4 molar ratio at 4°C overnight, and the CHIP-Fab sample was diluted in MP buffer (50 mM HEPES, 50 mM KCl, pH 7.4) to reach final concentration of about 80 nM of CHIP-Fab. 4 µL of protein sample was applied to a glow-discharged carbon-coated copper grid (Ted Pella Inc., Redding, CA, USA), washed with two drops of deionized water, stained with two drops of freshly prepared 0.75% uranyl formate, and the excess of liquid was blot off and dried under the vacuum line. The sample was imaged on a T12 microscope (FEI Company, Hillsboro, OR, USA) operated at 120 kV, and images were taken at a magnification of 30,000× using a TemF816 8 K × 8 K CMOS camera (TVIPS GmbH, Gauting, Germany) with a calibrated pixel size of 2.25 Å. Particle extraction and 2-dimensional classification were performed using RELION.

Fluorescence polarization (FP) binding assay

FP assays were run in 18 µL in a black 384 well low volume plate and read on a BioTek H4 multimode plate reader at room temperature. A 4× stock of CHIP (21.5 nM final) and a 4× stock

of CHIPOpt Tracer (FITC-AhxLWWPD, 1nM final) was made in FP buffer (HEPES pH7.4, 50mM KCl, 0.01% TritonX-100). The 2× Fab dilutions were prepared in CHIP Fab buffer (50 mM HEPES and 150 mM KCl, pH 7.4) in an 11 point serial dilution. CHIP and the CHIP Fab dilutions were mixed and incubated for 30 minutes at room temperature. CHIPOpt tracer was added and mixed. Reads were taken at 0 minutes and 20 minutes after substrate addition. Raw polarization (mP) data were plotted relative to $\log_{10}(\text{Fab})M$. Data was fit to the model for $\log(\text{antagonist})$ versus response (variable slope) in Graphpad Prism 9. To ensure changes in mP were not caused by Fabs interacting with CHIPOpt Tracer, a modified FP assay was performed. All steps remained the same, except the 4× CHIP stock was replaced with FP buffer.

In vitro ubiquitination assays

To evaluate CHIP's direct ubiquitination of substrates, 5× stock solutions were prepared comprising of (a) Ube1 (R&D Systems) + UbcH5c/UBE2D3 (R&D Systems) (400 nM Ube1 and 4 μM UbcH5c), (b) Ubiquitin (R&D Systems) (1 mM Ub), (c) CHIP+TauD421 (4 μM CHIP, 4 μM TauD421) and (d) ATP + MgCl₂ (10 mM ATP and 10 mM MgCl₂) in *in vitro* ubiquitination assay buffer (50 mM Tris pH 8.0, 15 mM NaCl). Fabs were diluted in CHIP Fab buffer to the appropriate 5× concentration. Fabs and CHIP were preincubated at room temperature for 30 minutes to allow for complexing prior to the ubiquitination assay. Reactions were assembled by combining 5 ul of each 5× stock for a final volume of 25 uL. Reactions were incubated at room temperature for 6 minutes and then stopped by the addition of 4× Laemlli loading dye+40 mM TCEP and a 5 minute incubation at 95 °C. Samples were run on onto 4–20% SDS-PAGE gradient gels (Bio-Rad). Ubiquitination was assessed by Western blot (Anti-CHIP Antibody, #2080, Cell Signaling Technologies; Anti-Myc Tag Antibody clone 4A6, #16-213, Sigma-Aldrich; Anti-Hsp70, #PA5-77828, Invitrogen) with antibodies diluted 1:1000. Quantification

was performed using Image Lab Software (Biorad), and statistics done using ANOVA testing in Graphpad Prism 9.

scFv reformatting

Reformatting of Fabs to scFvs for mammalian expression was based off previous a report.² A FLAG tag was added to the c-termini of all scFvs. All constructs synthesized (Twist Biosciences) were cloned into the pTwist-Efl alpha vector.

Cell culture

HEK293T cells and SK-MEL-28 cells were obtained from ATCC, while the NanoBit complementation assay cells were generous gifts from the Gestwicki lab (UCSF). All cells were cultured in Dulbecco's Modified Eagle Medium (DMEM) with a final concentration of 10% Fetal Bovine Serum (FBS) and 1% penicillin/streptomycin. Cultures were maintained at 37°C and 5% CO₂.

Transfections

HEK293T cells were transfected with scFv-coding constructs using TransIT-293 reagent (Mirus Bio, #2704) with standard protocols. SK-MEL-28 were transfected with Lipofectamine LTX reagent with Plus reagent using standard protocols (Invitrogen, #A12621).

NanoBit complementation assay

Luminescence assays were based on a modified version of previously described methods and cell line.¹³ Briefly, 10,000 cells/well were seeded into white 96-well plates coated with poly-L-lysine. While the cells were seeded, 100 ug/mL of doxycycline was added to the media to induce the expression of the NanoBit complementation assay components, and cells were transfected with scFv-coding constructs using Transit-293 reagent (Mirus Bio). At 24 hours post seeding, Nano-Glo live cell reagent (Promega) was prepared by diluting 1 volume of Nano-Glo Live Cell

Reagent into 19 volumes of Nano-Glo LCS buffer (12.5 uL/well). This was mixed with fresh Opti-Mem media (50 uL/well), for a total solution volume of 62.5 uL per well. Media was removed from cells and the solution was added to each well. Plates were incubated at room temperature for 5 minutes, and luminescence was read on a BioTek Synergy Neo2 using a 500 ms integration time. Uninduced reporter cells transfected with scFv plasmids were used to obtain background measurements, and these were used to normalize luminescence values. Statistics were run in Prism 9, using non-parametric T-tests to compare individual scFvs to the empty vector control.

Immunoprecipitation

HEK293T cells were seeded at a density of 2.5 million cells per plate in a 10cm plate and incubated overnight. The next day, cells were transfected with mammalian scFv expression constructs using Transit-293 (Mirus Bio). After a 24-hour incubation, cells were washed once with cold Dulbecco's phosphate-buffered saline, and then lysed with 1mL of cold IP lysis buffer (Pierce) supplemented with protease inhibitor (Roche). Wells were scraped and transferred to Eppendorf tubes and incubated on ice for 5 minutes. Samples were centrifuged at 4 °C, 15,000g for 15 minutes. Supernatant was collected and put into new tubes. Prior to immunoprecipitation, sample concentrations were normalized using a bicinchoninic acid assay (Pierce).

Input samples were set aside by mixing 48 uL of lysate with 16 uL of 4X Laemlli buffer supplemented with 40mM TCEP and were then incubated at 95 °C for 5 minutes. Denatured input samples were stored at -80°C. To co-immunoprecipitate CHIP, one mg of total protein for each sample were incubated with 50 uL/sample of washed Pierce™ Anti-DYKDDDDK Magnetic Agarose (Invitrogen, A36797) at 4°C overnight with rotation. The following day, flowthrough was collected, and beads were washed three times with the IP lysis buffer

supplemented with protease inhibitor. Proteins were eluted from beads by adding 60uL of 2x Laemlli buffer and incubating the samples at 95 °C for 5 min. Inputs, flowthroughs and elutions were run on Bis-Tris 4-20% gels (Invitrogen) and assessed by Western blot.

Western blotting

Gels were transferred onto PVDF membranes using an iBlot2 (Invitrogen), p0 cycle. Membranes were blocked with a solution containing 3% bovine serum albumin (BSA) in Tris buffered saline plus Tween20 (TBST) for 1 hour at room temperature. Primary antibodies (Anti-STUB1/CHIP Antibody, #ab134064, Abcam; Anti-B-Actin Antibody, #A2228, Sigma-Aldrich; Anti-Flag Tag, 14739, Cell Signaling Technology) were diluted 1:1,000-1:5000 in TBST+3%BSA and incubated at 4 °C overnight. Blots were washed 3 times with TBST. Secondary antibodies were diluted into TBST+3%BSA, added to the blots, and incubated at room temperature for 1 hour. Secondaries were removed, and blots washed three times with TBST before imaging on a Chemidoc (Bio-Rad). For immunoprecipitation samples, VeriBlot secondary (#ab131366, Abcam) was used to reduce heavy/light chain staining on the blots.

PDL-1 expression response to interferon-gamma stimulation

SK-MEL-28 cells were transfected with Lipofectamine LTX reagent and Plus reagent. At 24hours post transfection, media was replaced with normal growth media, or growth media supplemented with 25ng/mL interferon-gamma. One set of plates was collected at timepoint 0, and the second at 10 hours post media change. RNA was extracted using RNeasy Mini Kit (Qiagen, # 74104). RNA concentration was determined by nanodrop to normalize samples (20 ng of RNA per RT-qPCR reaction). RT-qPCR one-step reactions using the Luna universal probe one-step RT-qPCR kit (NEB, #E3006) were performed to assay for gene expression. Probes were purchased from Thermo Fisher (RPL13, Hs00744303_s1; PDL-1, Hs00204257_m1). PDL1

gene expression was normalized to RPL13 expression and compared to the negative control transfection using the $\Delta\Delta Ct$ approach. Statistics were performed in Prism 9.

1.6 Figures and Tables

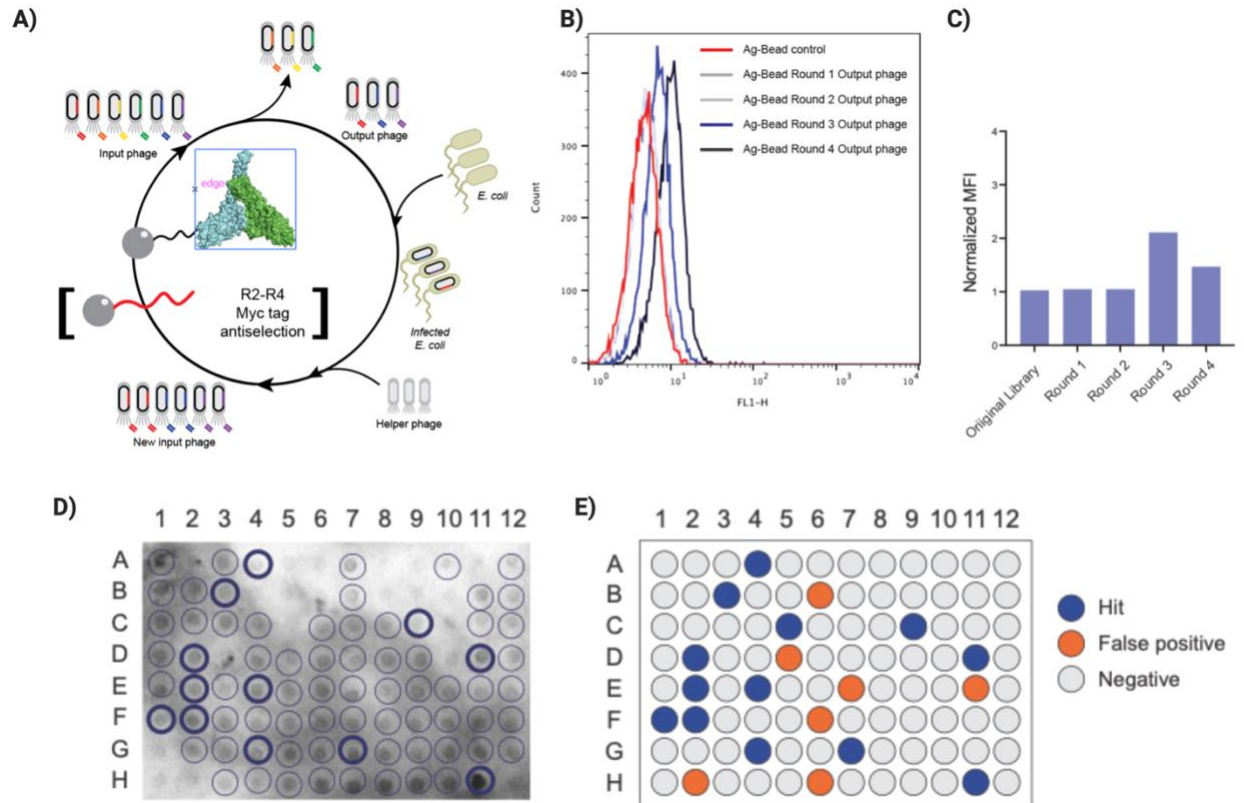


Figure 1.1: Biological panning identified multiple recombinant antibodies against CHIP

A) Four rounds of standard phage display biological panning were used to identify antibodies against CHIP. Rounds 2-4 had anti-Myc tag selections to reduce enrichment of non-CHIP specific phage. **B)** Output phage from each round were fluorescently labelled and assessed using flow cytometry to identify the round with the most enrichment for CHIP binders, indicated by the round with the furthest right shift in fluorescence. **C)** The mean fluorescence intensity (MFI) is the summary statistic to identify the round with the most enrichment for target binding phage. Round 3 has the most enrichment, and enrichment decreases in round 4. **D)** Via dot blot, around 80% of the colonies on this representative plate from round 3 are positive for Fabs. **E)** BIAS successfully identifies hits that have high affinity for CHIP but may have had high expression on the dot blot. Only 20 colonies are identified as positives, of which 13 have measurable affinity for CHIP.

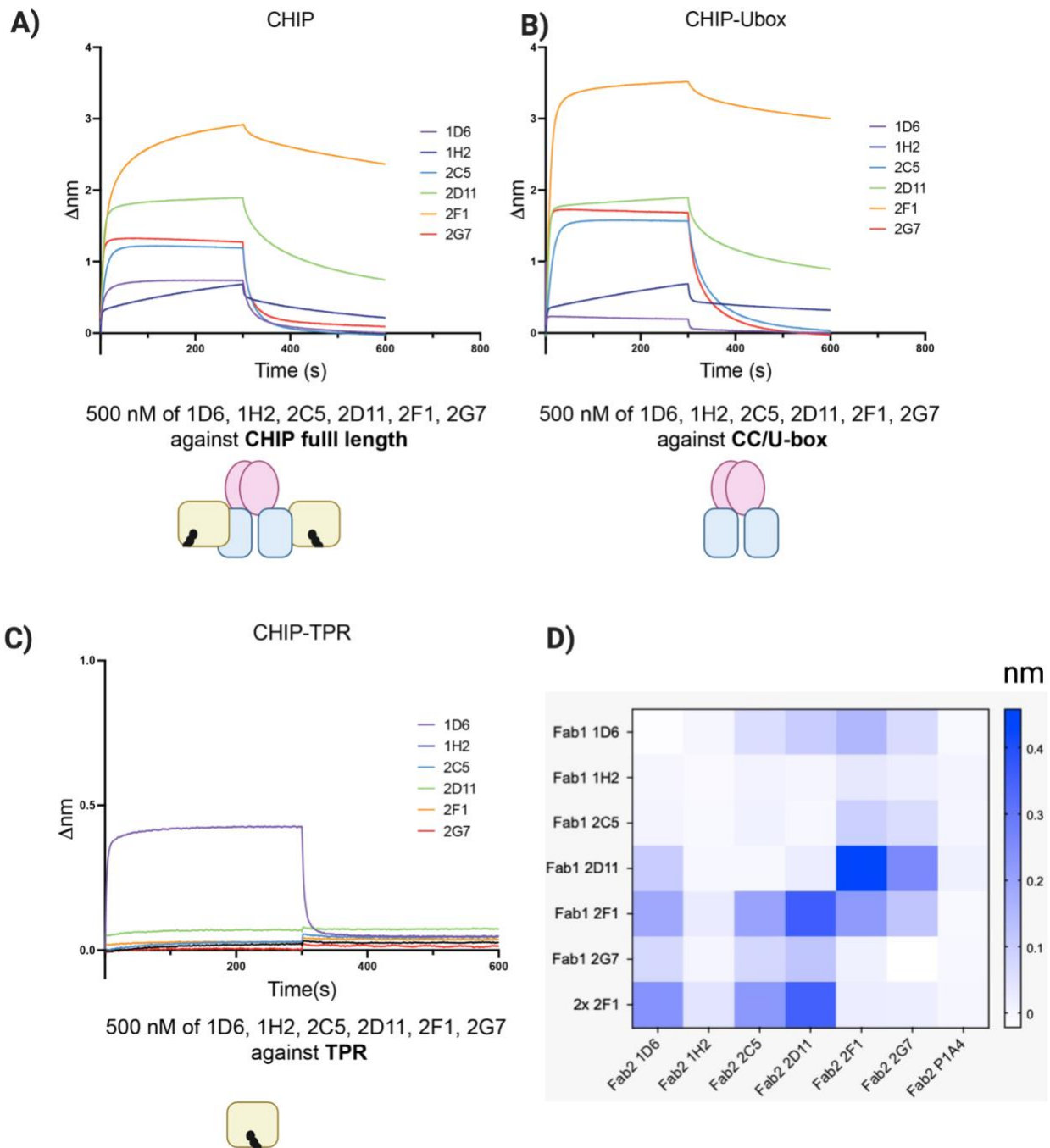


Figure 1.2: High affinity Fabs with varying epitopes were identified from round 3

A) Six Fabs were selected for further characterization based on their affinity for CHIP. **B)** All Fabs can bind to the UBox/CC region of CHIP, but D6 has a noticeable drop in affinity to the Ubox/CC compared to full-length CHIP. **C)** D6 has the highest affinity for TPR out of the tested Fabs. **D)** Overlapping or occluded epitopes were determined using competitive BLI. Fab pairs with more overlap in epitopes are annotated in white, while less epitope overlap is indicated by blue. Fab2 P1A4 is a control Fab for a different campaign and has affinity for CHIP, and therefore is expected to have no binding during these assays.

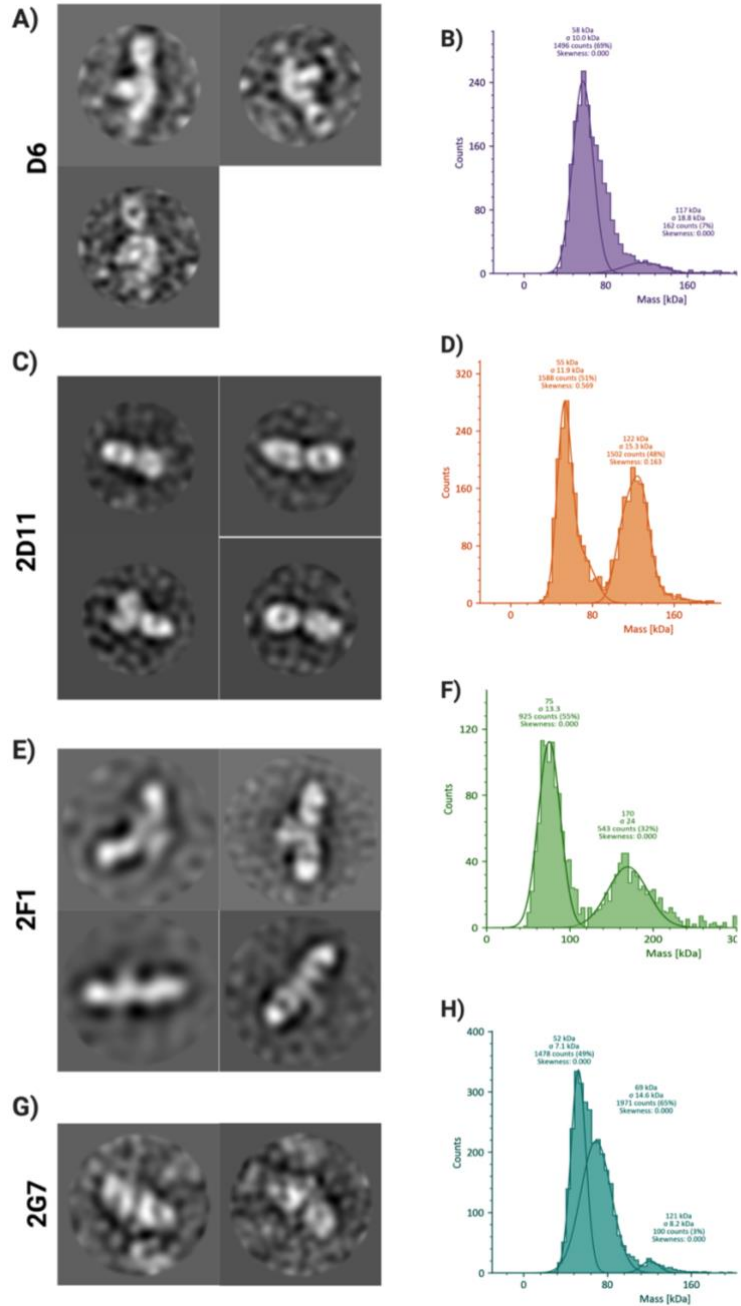


Figure 1.3: Negative stain and mass photometry provide insights into Fab binding modalities and epitopes

A) D6 mostly binds to the TPR based on negative stain. **B)** D6 has two peaks in the mass photometry. The first peak (58 kDa) is a mix of CHIP dimer and the second (117 kDa) corresponds to the MW of CHIP dimer+1 Fab. **C)** 2D11 negative stains indicate it binds in the CC region of CHIP. **D)** The first mass photometry peak for 2D11 (55 kDa) is a mix of CHIP dimer and Fab while the second (122 kDa) corresponds to the MW of CHIP dimer+1 Fab. **E)** Negative stain indicates two 2F1 Fabs bind near the junction of the TPR and the Ubox on a CHIP dimer. **F)** The second peak in the 2F1 mass photometry (170 kDa) corresponds to the molecular weight of 2 Fabs and one CHIP dimer. **G)** 2G7 negative stains indicate one Fab binds in the CC domain. **H)** 2G7 mass photometry shows the typical peaks (lower MW mix of CHIP dimer and free Fab, higher MW peak indicating one Fab with a CHIP dimer), but also has an intermediate peak (69 kDa) that would correspond to 1 CHIP monomer plus one Fab.

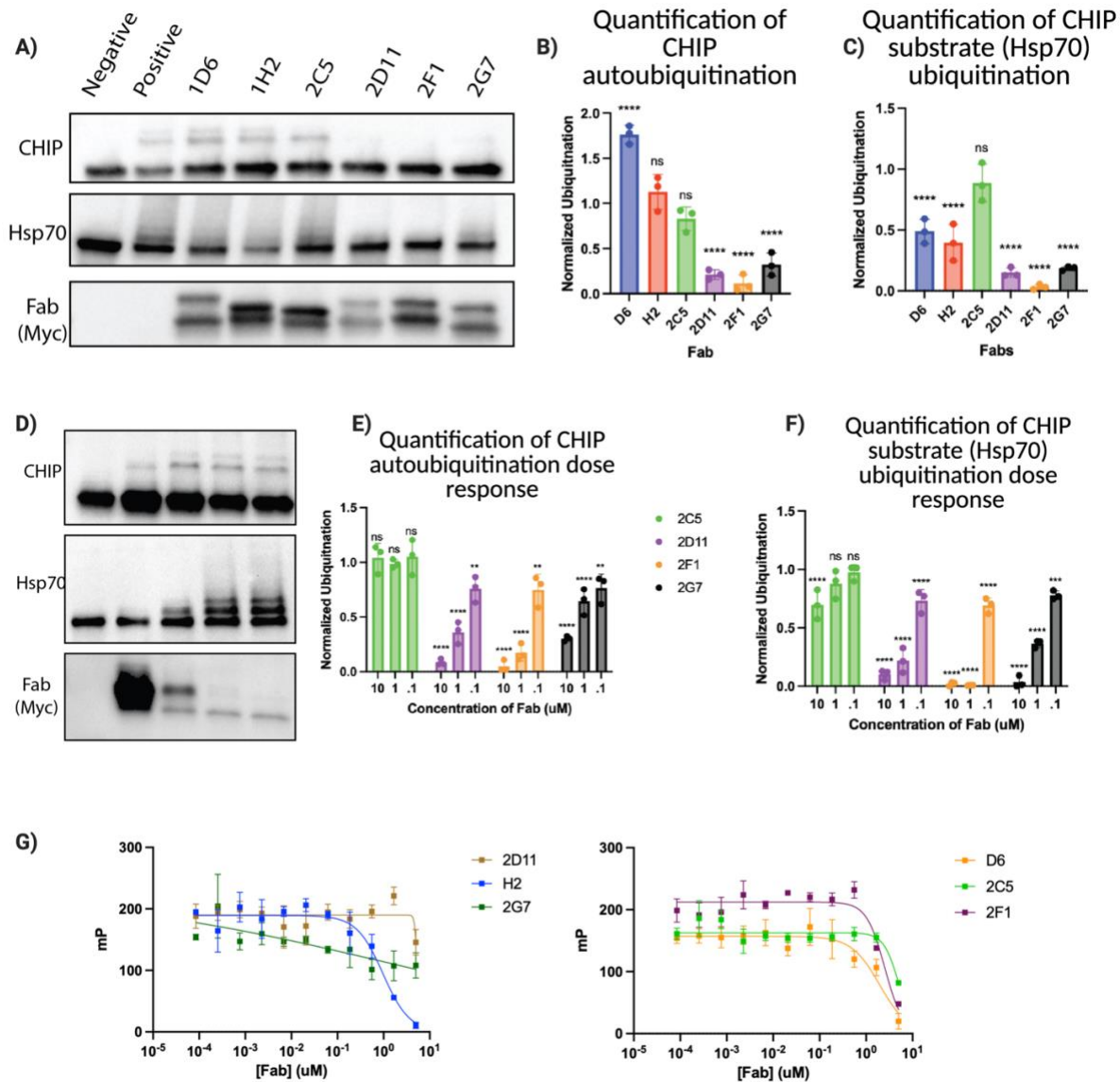


Figure 1.4: CHIP Fabs can inhibit CHIP E3 function and CHIP binding activity

A) Representative blot of CHIP *in vitro* ubiquitination assays. Reactions were supplemented with 5 μ M of CHIP Fabs to screen for inhibitory activity. All CHIP Fabs show two bands when blotted for using an anti-Myc antibody, seemingly unrelated to ubiquitination of the Fab. **B)** Quantification of the ubiquitination reactions shows D6 increases CHIP autoubiquitination, while 2D11, 2F1, and 2G7 inhibit autoubiquitination. **C)** All Fabs except 2C5 inhibit substrate (Hsp70) ubiquitination. **D)** Representative blot showing dose-dependency of inhibition of ubiquitination reactions. **E)** Three most ubiquitination inhibitory Fabs were brought forward for dose response testing, along with 2C5 to act as a negative control. Inhibition of autoubiquitination was dose dependent for 2D11, 2F1, and 2G7. **F)** Three of the Fabs (2D11, 2F1, and 2G7) show inhibition of CHIP substrate (Hsp70) ubiquitination in a dose dependent manner. 2C5 only shows inhibition in the highest concentration tested (10 μ M). **G)** Fabs were tested for inhibition of CHIP substrate binding using fluorescence polarization against CHIP-Opt, a peptide with optimized affinity for CHIP TPR. Three Fabs (D6, H2, and 2F1) have IC₅₀ values less than 5 μ M in this assay.

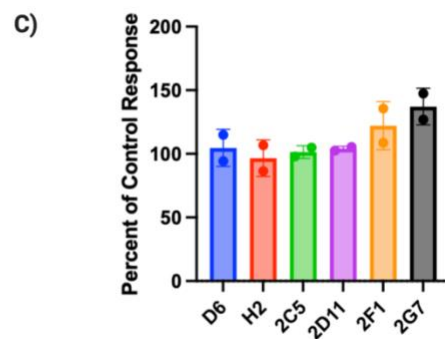
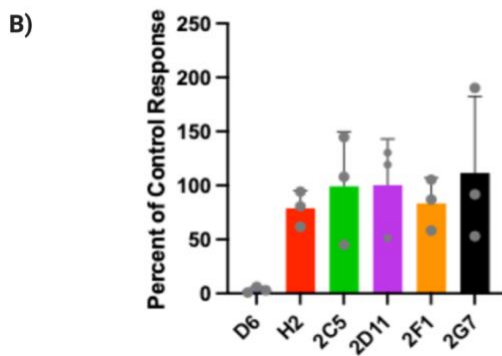
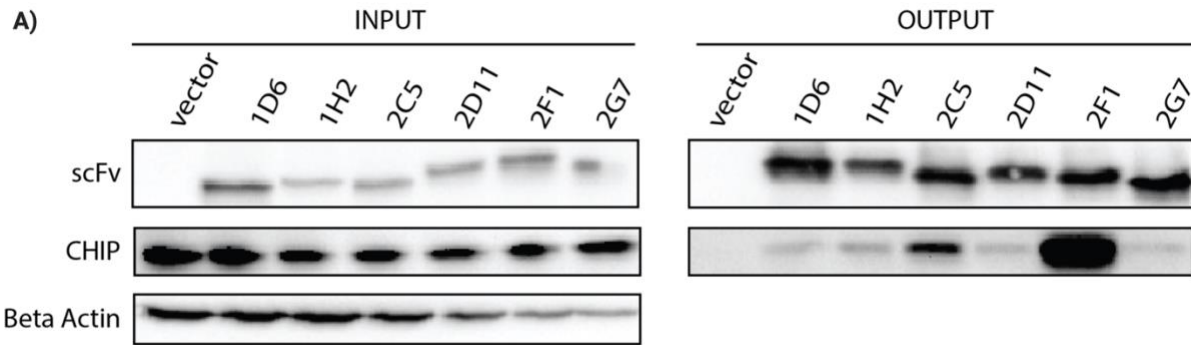
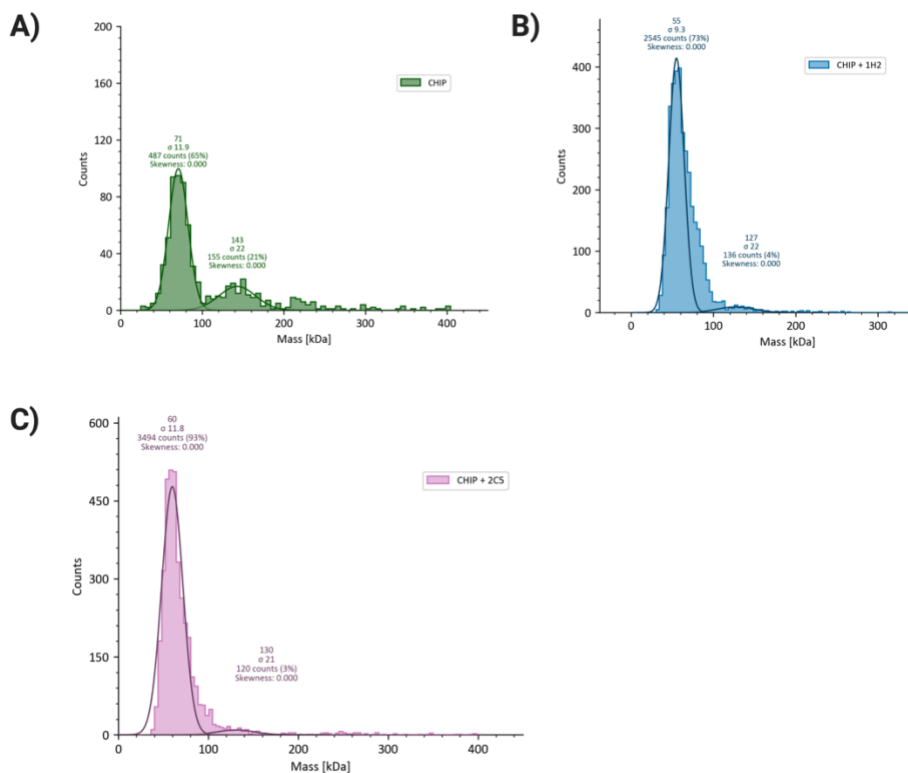


Figure 1.5: scFv versions of the recombinant antibodies against CHIP are able to bind and inhibit cellular CHIP when overexpressed in cells

A) CHIP Fabs were reformatted into scFvs and expressed in mammalian cells by transient transfection. CHIP co-immunoprecipitated with the scFvs during immunoprecipitation against a tag on the scFv. **B)** Nano-Bit complementation assay shows on D6 inhibits substrate binding in cells. **C)** Preliminary data suggest 2F1 and 2G7 can inhibit CHIP ubiquitination in cells. CHIP was recently described as stabilizing IFNGR1. After stimulating SK-MEL-28 cells with IFN-gamma, expression of 2F1 and 2G7 scFvs led to higher PDL-1 (an interferon response element) transcription. Plotted is RNA levels of PDL-1, normalized to RPL13 expression and then normalized to the negative control response.



Supplementary Figure 1.1: Additional mass photometry.

A) CHIP alone shows two peaks, one at 71 kDa (approximate molecular weight of CHIP dimer) and one at 143 kDa (approximate MW of CHIP tetramer). CHIP is known to oligomerize under these conditions. **B)** H2 has two peaks. The first peak (55 kDa) is a mix of CHIP dimer and the second (127 kDa) corresponds to the MW of CHIP dimer+1 Fab. **C)** 2C5 has a similar profile to H2, with slightly shifted peaks. The first peak (50 kDa) is a mix of CHIP dimer and Fab while the second (130 kDa) corresponds to the MW of CHIP dimer+1 Fab.

Table 1.1: Kd determined by BLI of each Fab to CHIP or domains with Fab on the tip

	CHIP		UBOX+CC		TPR	
	<u>Kd (nM)</u>	<u>R²</u>	<u>Kd (nM)</u>	<u>R²</u>	<u>Kd (nM)</u>	<u>R²</u>
D6	140 ± 18	.9747	1300 ± 170	.99	300 ± 24	.9969
H2	210 ± 50	.9512	N/A	N/A	390 ± 90	.9548
2C5	120 ± 18	.9725	480 ± 97	.9525	450 ± 78	.9711
2D11	27 ± 1.9	.9855	100 ± 13	.9578	N/A	N/A
2F1	28 ± 2	.9812	63 ± 7.2	.9732	N/A	N/A
2G7	54 ± 4.1	.9885	90 ± 6.6	.99	N/A	N/A

1.7 References

- (1) Ravalin, M.; Theofilas, P.; Basu, K.; Opoku-Nsiah, K. A.; Assimon, V. A.; Medina-Cleghorn, D.; Chen, Y.-F.; Bohn, M. F.; Arkin, M.; Grinberg, L. T.; Craik, C. S.; Gestwicki, J. E. Specificity for Latent C Termini Links the E3 Ubiquitin Ligase CHIP to Caspases. *Nat Chem Biol* **2019**, *15* (8), 786–794. <https://doi.org/10.1038/s41589-019-0322-6>.
- (2) Buetow, L.; Huang, D. T. Structural Insights into the Catalysis and Regulation of E3 Ubiquitin Ligases. *Nat Rev Mol Cell Biol* **2016**, *17* (10), 626–642. <https://doi.org/10.1038/nrm.2016.91>.
- (3) McDonough, H.; Patterson, C. CHIP: A Link between the Chaperone and Proteasome Systems. *Cell Stress Chaper* **2003**, *8* (4), 303. [https://doi.org/10.1379/1466-1268\(2003\)008<0303:CALBTC>2.0.CO;2](https://doi.org/10.1379/1466-1268(2003)008<0303:CALBTC>2.0.CO;2).
- (4) Murata, S.; Minami, Y.; Minami, M.; Chiba, T.; Tanaka, K. CHIP Is a Chaperone-Dependent E3 Ligase That Ubiquitylates Unfolded Protein. *EMBO Rep.* **2001**, *2* (12), 1133–1138. <https://doi.org/10.1093/embo-reports/kve246>.
- (5) Qian, S.-B.; McDonough, H.; Boellmann, F.; Cyr, D. M.; Patterson, C. CHIP-Mediated Stress Recovery by Sequential Ubiquitination of Substrates and Hsp70. *Nature* **2006**, *440* (7083), 551–555. <https://doi.org/10.1038/nature04600>.
- (6) Balaji, V.; Müller, L.; Lorenz, R.; Kevei, É.; Zhang, W. H.; Santiago, U.; Gebauer, J.; Llamas, E.; Vilchez, D.; Camacho, C. J.; Pokrzywa, W.; Hoppe, T. A Dimer-Monomer Switch Controls CHIP-Dependent Substrate Ubiquitylation and Processing. *Molecular Cell* **2022**, S1097276522007560. <https://doi.org/10.1016/j.molcel.2022.08.003>.
- (7) Apriamashvili, G.; Vredevoogd, D. W.; Krijgsman, O.; Bleijerveld, O. B.; Ligtenberg, M. A.; de Bruijn, B.; Boshuizen, J.; Traets, J. J. H.; D’Empaire Altimari, D.; van Vliet, A.; Lin,

- C.-P.; Visser, N. L.; Londino, J. D.; Sanchez-Hodge, R.; Oswalt, L. E.; Altinok, S.; Schisler, J. C.; Altelaar, M.; Peeper, D. S. Ubiquitin Ligase STUB1 Destabilizes IFN γ -Receptor Complex to Suppress Tumor IFN γ Signaling. *Nat Commun* **2022**, *13* (1), 1923. <https://doi.org/10.1038/s41467-022-29442-x>.
- (8) Ng, S.; Lim, S.; Sim, A. C. N.; Mangadu, R.; Lau, A.; Zhang, C.; Martinez, S. B.; Chandramohan, A.; Lim, U.-M.; Ho, S. S. W.; Chang, S. C.; Gopal, P.; Hong, L. Z.; Schwaid, A.; Fernandis, A. Z.; Loboda, A.; Li, C.; Phan, U.; Henry, B.; Partridge, A. W. STUB1 Is an Intracellular Checkpoint for Interferon Gamma Sensing. *Sci Rep* **2022**, *12* (1), 14087. <https://doi.org/10.1038/s41598-022-18404-4>.
- (9) Koochaki, S. H. J.; Słabicki, M.; Lumpkin, R.; Zou, C.; Belizaire, R.; Fischer, E. S.; Ebert, B. L. A STUB1 Ubiquitin Ligase/CHIC2 Protein Complex Negatively Regulates the IL-3, IL-5, and GM-CSF Cytokine Receptor Common β Chain (CSF2RB) Protein Stability. *Journal of Biological Chemistry* **2022**, *298* (10), 102484. <https://doi.org/10.1016/j.jbc.2022.102484>.
- (10) Okiyoneda, T.; Barriere, H.; Bagdany, M.; Rabeh, W. M.; Du, K.; Hohfeld, J.; Young, J. C.; Lukacs, G. L. Peripheral Protein Quality Control Removes Unfolded CFTR from the Plasma Membrane. *Science* **2010**, *329* (5993), 805–810. <https://doi.org/10.1126/science.1191542>.
- (11) Zhang, S.; Hu, Z.; Mao, C.; Shi, C.; Xu, Y. CHIP as a Therapeutic Target for Neurological Diseases. *Cell Death Dis* **2020**, *11* (9), 727. <https://doi.org/10.1038/s41419-020-02953-5>.
- (12) Békés, M.; Langley, D. R.; Crews, C. M. PROTAC Targeted Protein Degradation: The Past Is Prologue. *Nat Rev Drug Discov* **2022**, *21* (3), 181–200. <https://doi.org/10.1038/s41573-021-00371-6>.

- (13) Nadel, C. M.; Ran, X.; Gestwicki, J. E. Luminescence Complementation Assay for Measurement of Binding to Protein C-Termini in Live Cells. *Analytical Biochemistry* **2020**, *611*, 113947. <https://doi.org/10.1016/j.ab.2020.113947>.
- (14) Ng, S.; Brueckner, A.; Bahmanjah, S.; Deng, Q.; Johnston, J.; Ge, L.; Duggal, R.; Habulihaz, B.; Barlock, B.; Ha, S.; Sadruddin, A.; Yeo, C.; Strickland, C.; Peier, A.; Henry, B.; Sherer, E.; Partridge, A. *Discovery and Structure-Based Design of Macrocyclic Peptides Targeting STUB1*; preprint; Chemistry, 2021. <https://doi.org/10.26434/chemrxiv-2021-1108b>.
- (15) Choi, W. H.; Yun, Y.; Park, S.; Jeon, J. H.; Lee, J.; Lee, J. H.; Yang, S.-A.; Kim, N.-K.; Jung, C. H.; Kwon, Y. T.; Han, D.; Lim, S. M.; Lee, M. J. Aggresomal Sequestration and STUB1-Mediated Ubiquitylation during Mammalian Proteaphagy of Inhibited Proteasomes. *Proc Natl Acad Sci USA* **2020**, *117* (32), 19190–19200. <https://doi.org/10.1073/pnas.1920327117>.
- (16) Kanack, A. J.; Olp, M. D.; Newsom, O. J.; Scaglione, J. B.; Gooden, D. M.; McMahon, K.; Smith, B. C.; Scaglione, K. M. Chemical Regulation of the Protein Quality Control E3 Ubiquitin Ligase C-Terminus of Hsc70 Interacting Protein (CHIP). *ChemBioChem* **2022**, *23* (6). <https://doi.org/10.1002/cbic.202100633>.
- (17) Böldicke, T. Therapeutic Potential of Intrabodies for Cancer Immunotherapy: Current Status and Future Directions. *Antibodies* **2022**, *11* (3), 49. <https://doi.org/10.3390/antib11030049>.
- (18) Marschall, A. L. J.; Dübel, S. Antibodies inside of a Cell Can Change Its Outside: Can Intrabodies Provide a New Therapeutic Paradigm? *Computational and Structural Biotechnology Journal* **2016**, *14*, 304–308. <https://doi.org/10.1016/j.csbj.2016.07.003>.

- (19) Zhang, C.; Ötjengerdes, R. M.; Roewe, J.; Mejias, R.; Marschall, A. L. J. Applying Antibodies Inside Cells: Principles and Recent Advances in Neurobiology, Virology and Oncology. *BioDrugs* **2020**, *34* (4), 435–462. <https://doi.org/10.1007/s40259-020-00419-w>.
- (20) Binning, J. M.; Smith, A. M.; Hultquist, J. F.; Craik, C. S.; Caretta Cartozo, N.; Campbell, M. G.; Burton, L.; La Greca, F.; McGregor, M. J.; Ta, H. M.; Bartholomeeusen, K.; Peterlin, B. M.; Krogan, N. J.; Sevillano, N.; Cheng, Y.; Gross, J. D. Fab-Based Inhibitors Reveal Ubiquitin Independent Functions for HIV Vif Neutralization of APOBEC3 Restriction Factors. *PLOS Pathogens* **2018**, *14* (1), e1006830. <https://doi.org/10.1371/journal.ppat.1006830>.
- (21) Wang, C.-I.; Yang, Q.; Craik, C. S. Isolation of a High Affinity Inhibitor of Urokinase-Type Plasminogen Activator by Phage Display of Ecotin. *Journal of Biological Chemistry* **1995**, *270* (20), 12250–12256. <https://doi.org/10.1074/jbc.270.20.12250>.
- (22) Goodwin, M. S.; Sinyavskaya, O.; Burg, F.; O’Neal, V.; Ceballos-Diaz, C.; Cruz, P. E.; Lewis, J.; Giasson, B. I.; Davies, P.; Golde, T. E.; Levites, Y. Anti-Tau ScFvs Targeted to the Cytoplasm or Secretory Pathway Variably Modify Pathology and Neurodegenerative Phenotypes. *Molecular Therapy* **2021**, *29* (2), 859–872. <https://doi.org/10.1016/j.ymthe.2020.10.007>.
- (23) Messer, A.; Butler, D. C. Optimizing Intracellular Antibodies (Intrabodies/Nanobodies) to Treat Neurodegenerative Disorders. *Neurobiology of Disease* **2020**, *134*, 104619. <https://doi.org/10.1016/j.nbd.2019.104619>.
- (24) Duriseti, S.; Goetz, D. H.; Hostetter, D. R.; LeBeau, A. M.; Wei, Y.; Craik, C. S. Antagonistic Anti-Urokinase Plasminogen Activator Receptor (UPAR) Antibodies Significantly Inhibit UPAR-Mediated Cellular Signaling and Migration. *Journal of*

Biological Chemistry **2010**, 285 (35), 26878–26888.

<https://doi.org/10.1074/jbc.M109.077677>.

**Chapter 2: HHV-8's ORF28 interacts with host-protein CHIP to mediate
ubiquitination of host proteins**

2.1 Abstract

CHIP is a host E3 ubiquitin ligase that is canonically known to mark misfolded chaperone clients for degradation. However, recent publications indicate CHIP can interact with and ubiquitinate substrates in a chaperone-independent manner. Hsp-independent interactions were computationally predicted based on empirically derived CHIP binding affinities, and Human Herpesvirus-8's ORF28 was predicated to have a high affinity for CHIP. We demonstrate CHIP associates with ORF28 in the context of overexpression, and ORF28 expression leads CHIP to relocalize to cell membranes. Interaction partners and ubiquitination substrates were identified via IP-MS and ubiquitin remnant profiling, suggesting this interaction may lead to ubiquitination of host proteins during viral replication. While similar in principle and function to the viral E3 ubiquitin ligases K3/K5, this interaction may represent a novel mechanism of boosting viral fitness in HHV-8 by ubiquitination of host proteins by a host E3.

2.2 Introduction

E3 ubiquitin ligases regulate proteostasis by recognizing and ubiquitinating protein substrates. Ubiquitination leads to substrate degradation or alteration in localization.¹⁻³ The end binding subset of E3 ubiquitin ligases recognize N-termini (N-degron pathways) or C-termini (C-degron pathways) of proteins and protein fragments. While N-degron pathways have a substantial body of literature, C-degrons have been comparatively undescribed until recent studies involving Cullin-RING E3 ubiquitin ligases and Carboxyl-terminus of Hsp70-Interacting Protein (CHIP).¹⁻⁴ CHIP's canonical function is chaperone dependent, relying on CHIP binding to the C-termini of heat shock protein 70 and 90 (Hsp70 and 90) to ubiquitinate misfolded clients, as well as regulate Hsp levels after stress response.^{5,6}

The paradigm of CHIP's E3 function being chaperone-dependent is challenged by data indicating the specificity of CHIP binding compasses C-termini beyond Hsps. Many of these C-termini are formed through proteolytic cleavage by caspases, including caspase-6.⁴ CHIP can bind to and inhibit the active form of caspase-6, indicating the production of Hsp-independent CHIP interactors may be at least partially self-regulating. These interactions suggest CHIP may mediate ubiquitination in an undescribed C-degron pathway occurring in parallel to CHIP's canonical, Hsp-dependent pathway. Based on empirical binding data, 2700 new, Hsp-independent CHIP interactors were predicted beyond caspase-6 in the human proteome, suggesting this pathway may impact a variety of diseases states, including viral replication.

CHIP interactions with viral proteins have been shown to play a role in the life cycle of some viruses, including human immunodeficiency virus (HIV) and hepatitis B virus (HBV). In HIV, CHIP interacts with the viral protein Vif, which is necessary for the virus to replicate efficiently. This interaction promotes Vif's degradation, which ultimately leads to reduced HIV replication.⁷ In hepatitis B virus, CHIP has been shown to clear the viral protein HBc, one of the major structural proteins of HBV, after HBc is aggregated by inhibitor treatment. Increased expression of CHIP was also shown to help reduce levels of long term infection when combined with anti HBc therapy.⁸ Overall, the precise roles of CHIP in viral lifecycles are still under investigation.

Of the predicted CHIP interactors, the viral protein ORF28 from Human herpesvirus-8 (HHV-8) has one of the highest predicted affinities for CHIP. ORF28 is predicted to be a single-pass membrane protein, with an extracellular N-terminus and a cytoplasmic C-terminus.

Intriguingly, ORF28 is one of the few proteins where the anticipated CHIP interaction site is the coded C-terminus, as most interaction sites require the release of neo-C-termini by proteases.

ORF28 is expressed in the late lytic-cycle, meaning it is expressed during the replicative phase of

the virus.⁹ One study suggests that ORF28 in the closely related MHV68 is non-essential for replication, and may be involved in the formation of the viral tegument, the layer of proteins that surrounds the virus particle.¹⁰ Similarly, previous non-peer reviewed work suggests that ORF28 is heavily glycosylated, can become part of the viral tegument, and is not essential for viral replication.¹¹ However, further research is needed to fully understand the molecular mechanisms underlying ORF28's role in HHV-8's lifecycle.

Three related viral proteins suggest the ORF28+CHIP interaction may regulate host immune response against cells undergoing active viral replication. HHV-8 is closely related to Epstein-Barr virus, and the positional homolog of ORF28 in Epstein-Barr virus is gp150, a membrane glycoprotein that functions as an immune evasin. Gp150 increases immune evasion in infected cells by blocking recognition of surface proteins via the heavily glycosylated N-terminus.¹² In the HHV-8 genome, there are two viral E3 ubiquitin ligases (K3 and K5), both of which comprise of a membrane spanning domain and an E3 domain. These viral proteins ubiquitinate antigen presenting proteins to prevent immune recognition of cells undergoing active viral replication.^{13,14} These proteins bear functional, structural, and positional similarities to the CHIP+ORF28 complex, suggesting it may also play a role in immune regulation by ubiquitinating surface proteins.

Surface protein ubiquitination is an activity associated with both herpesviruses and CHIP.^{15,16} For example, HHV-8 has multiple mechanisms of reducing major histocompatibility complex I (MHC-I) localization to the cell surface, including two afore-mentioned viral E3 ubiquitin ligases.^{13,14} Multiple membrane proteins are regulated by CHIP, either during folding in the ER or after localization to the plasma membrane. Canonically, CHIP is known to regulate CFTR, and some cases of cystic fibrosis are caused by slower folding CFTR variants being

cleared by CHIP prior to adopting the proper conformation.¹⁷ On an immune response level, CHIP is implicated in regulating CSF2RB and IFNGR1. CHIP interacts with CHIC2, a host surface protein, that has a CHIP compatible C-terminus like ORF28. This interaction was recently determined to regulate the IL-3, IL5, and CM-CSF cytokine receptor common β -chain, CSF2RB. The CHIP+CHIC2 interaction prevents accumulation of receptors at the cell surface during periods of low cytokine levels, preventing premature cellular response to cytokines.¹⁸ CHIP is shown to negatively regulate IFNGR1.^{19,20} These examples of CHIP/HHV-8 modulation of immune related surface proteins imply the CHIP+ORF28 interaction may modulate ubiquitination of membrane proteins, leading to changes in protein levels on the cell surface.

With ORF28 acting as a transmembrane domain, and CHIP functioning as an E3 in a chaperone independent manner, the interaction between ORF28 and CHIP may function in a similar manner to K3/K5. When ORF28 is overexpressed, CHIP associates with ORF28, and colocalizes at the cell membrane with ORF28. Next, host interaction partners were identified via IP-MS and ubiquitination substrates by ubiquitin remnant profiling. These hits suggest this interaction enables remodeling of the proteome during a phase of viral infection that is distinct from when K3/K5 are active. While similar in principle and function to the viral E3 ubiquitin ligases K3/K5, this interaction may represent a novel mechanism of increasing viral replication in HHV-8 by using a host E3 to ubiquitinate host proteins.

2.3 Results

Identification of ORF28 as a potential CHIP binding partner

Potential CHIP interactors are identified by an algorithm that calculates the likelihood of an interaction occurring. This summary statistic known as a CHIP-score uses the predicted affinity for CHIP-TPR of a given five-peptide sequence in a protein, combined with the

likelihood of the peptide sequence being C-terminally accessible by either proteolytic cleavage or translation. When applying this algorithm to proteins from human viruses, around 25 proteins have a CHIP score exceeding that of Hsp90, the lower affinity CHIP co-chaperone canonically known to interact with CHIP (**Figure 2.1a**). The top scoring hit is ORF28, a small membrane protein from HHV-8. Intriguingly, ORF28 does not require proteolytic release of its predicted CHIP binding site, an abnormality as most CHIP sites require release by a caspase. ORF28 itself has no attributed function and is a single-pass transmembrane helix with a heavily glycosylated N-terminus (**Figure 2.1b**).

To examine if this predicted interaction truly occurs, CHIP's affinity of the six C-terminal amino acids of ORF28 was determined via fluorescence polarization. The IC_{50} of 16 nM translates to a K_i of around .5 nM, indicating the C-terminus of ORF28 has a strong affinity for the CHIP binding domain (**Figure 2.1c**). Next, analysis of previously published affinity purification-mass spectrometry data indicates that ORF28 has significantly more unique CHIP peptides associated with it than any other tested HHV-8 ORF (**Figure 2.1d**). Together, these studies indicate the C-terminus of ORF28 has high affinity for CHIP. Additionally, the mass spectrometry results suggest ORF28 can outcompete endogenous CHIP binding partners, at least in the context of overexpression in HEK293T cells.

ORF28 and CHIP interact when ORF28 is overexpressed HEK293T cells

Next, the ability of CHIP to interact with ORF28 in cells where there is a high concentration of competing CHIP interactors like Hsps was examined. To do so, constructs coding for ORF28 with an N-terminal, extracellular HA tag (HAORF28) and the same construct with the CHIP-compatible C-terminus removed (HAORF28 Δ C-term) were generated (**Figure 2.1b**). When immunoprecipitating against the HA tag on the ORF28 constructs, CHIP co-

immunoprecipitated with HAORF28, and not HAORF28 Δ C-term (**Figure 2.2a**). This indicates the interaction between ORF28 and CHIP occurs in cells, that ORF28 can outcompete other CHIP interactors like Hsps, and the interaction is dependent on the predicted CHIP interaction site on the C-terminus of ORF28. Next, ORF28 and CHIP localization was determined. Via immunofluorescence HAORF28 and HAORF28 Δ C-term localized to cell membranes, indicating the addition of the HA-tag did not impact the presumed localization of ORF28. Upon examination of CHIP localization, only HAORF28 substantially recruited CHIP to the cell membranes (**Figure 2.2b**). While CHIP binds to ORF28 in a C-terminal dependent manner, and relocates to the cell membrane when HAORF28 is expressed, these data do not provide insights into the function of this interaction.

Assessment of CHIP-mediated ubiquitination of ORF28 and host surface proteins

Based on previous studies, CHIP's interaction with ORF28 has the potential to directly regulate ORF28 protein levels, as well as levels of neighboring membrane proteins without CHIP directly binding to the target. Preliminary assessment of first focused on the expression and stability of HAORF28 and HAORF28 Δ C-term. HAORF28 protein levels are lower than HAORF28 Δ C-term, suggesting ORF28 may be degraded by CHIP-mediated mechanisms. CHIP is capable of clearing membrane proteins through both ER associated degradation, preventing the trafficking of membrane proteins to the cell surface, or by ubiquitinating membrane proteins on the cell surface, leading the membrane proteins to be internalized and degraded in the lysosome. Only lysosomal inhibition increases the amount of HAORF28 and HAORF28 Δ C-term protein (**Figure 2.3a**). This result signals CHIP+ORF28's main mechanism of clearance is not through ER associated degradation, and instead, the interaction ubiquitinates proteins after they localize

to the cell membrane, similar to the CHIC2+CHIP interaction mediating ubiquitination of adjacent CSF2RB on the cell surface.

The resemblance the CHIP+ORF28 complex bears to the K3/K5 proteins in HHV-8 suggests the interaction may alter levels of surface proteins as well, albeit in a later portion of the viral life cycle compared to K3/K5. MHC-I and IFNGR1 levels were assayed after overexpression of HAORF28 and HAORF28 Δ C-term. These two host proteins were chosen for preliminary focus as MHC-I protein levels are reduced by K3/K5 to reduce immune response against replicating cells, and because of CHIP's role in IFNGR1 stability. When HAORF28 is expressed, there are reduced levels of IFNGR1 and MHC-I compared to the vector control. HAORF28 Δ C-term expression does not negatively impact MHC-I levels but does reduce IFNGR1 levels slightly (**Figure 2.3b**). These trends suggest the ORF28+CHIP interaction may be remodeling surface proteins to regulate host immune responses through two mechanisms: reduction of antigen presentation and prevention of interferon response. To examine further roles of the CHIP+ORF28 complex, non-biased identification of interaction partners was required.

Non-biased identification of ORF28-CHIP interaction partners and ubiquitination substrates

While HAORF28 reduces expression of two immune related proteins, non-biased identification of substrates via proteomics was also performed to identify novel host interactions. Both immunoprecipitation-mass spectrometry (IP-MS) and ubiquitin remnant profiling were used to identify potential ubiquitination targets of the CHIP+ORF28 interaction. First, IP-MS was performed to identify direct interactions of the CHIP+ORF28 complex. This method pulls direct interaction partners of the complex, helping identify semi-stable, host-protein interaction partners that may be ubiquitinated due to forced proximity to CHIP (**Table 2.1**). CHIP is the hit with the highest enrichment and lowest p-value (**Figure 2.4a**). Examining the proteins enriched

in the HAORF28 samples and the HA (negative control) samples, there are 1342 proteins that are present in both samples, 62 that only appear in the negative control, and 144 that are only in the HAORF28 samples (**Figure 2.4b**). The proteins that only appear in the HAORF28 and not in the negative control have an enrichment value of NA, as the fold change over undetected cannot be calculated (**Table 2.1**). To visualize the enriched proteins and how they interact, a network connecting the hits based on curated datasets or experimental data was generated using STRING (**Figure 2.4c**). The network generated by hits enriched in the HAORF28 IP-MS have significantly more interactions than expected (32 in network vs 12 expected, p-value 1.84e-06). These proteins show an increase in enrichment for processes related to mRNA splicing, and SUMOylation, both of which are important processes for HHV-8 replication.²¹⁻²³

Given the transient nature of ubiquitination interactions, IP-MS may not capture all relevant ubiquitination targets. After CHIP is recruited to the cell surface, it may ubiquitinate proteins without CHIP or ORF28 stably binding to the substrate. Thus, ubiquitin remnant profiling was used to examine ubiquitination substrates and sites to provide insights into more transient interactions. First, the proteins and ubiquitination sites with increased ubiquitination in the HAORF28 samples were examined (**Table 2.2**). Via network analysis, the proteins with increased ubiquitination when HAORF28 is expressed significantly more interactions (104 in network vs 51 expected, p-value 4.85e-11) than a random set of genes (**Figure 2.5a**). While the most interesting pathway enrichments are from the GO database instead of Reactome for the ubiquitin remnant profiling hits, multiple catabolic process pathways are enriched, as well as proteasomal pathways (**Figure 2.5b**). This is enrichment for similar functional pathways is particularly striking given there is no overlap in significant hits between the IP-MS and ubiquitin remnant profiling hits.

The sites with reduced ubiquitination were also examined (**Table 2.3**). These proteins form a network with significantly more interactions than expected (20 connections in network vs 11 expected, p-value 6.62 e-3), although many of these interactions and the enriched pathways are driven by well described relationships (**Figure 2.5c**). Here, pathway analysis proved less fruitful, as the majority of enriched Reactome pathways were driven by the proteasomal subunit hits (**Figure 2.5d**). Despite the significant increase in network connections among the downregulated ubiquitination sites, these hits overall do not seem to have a high amount of biological interest.

2.4 Discussion

These data indicate that CHIP binds to the C-terminus of ORF28 as predicted. This interaction changes the ubiquitination substrates of CHIP when ORF28 is overexpressed in HEK293T cells. While initial focus was on membrane immune proteins due to the similarity ORF28 and the CHIP+ORF28 complex bear to other known viral proteins that clear immune related cells, proteomics data indicate this interaction could be reducing catabolism and proteasomal degradation during the late lytic phase of viral replication. If these proteomics hits prove to be correct, this would suggest that instead of acting as a mechanism of immune evasion to protect cells with actively replicating virus, ORF28 is acting as a mechanism of reducing the clearance of viral proteins when there are high levels of viral proteins in cells. Further studies in an HHV-8 relevant cell line will determine if the catabolism related processes identified by proteomics or the immune related proteins identified by literature searching are the primary ubiquitination targets of the CHIP+ORF28 interaction.

While the preliminary data indicates the potential of this interaction performing an as of yet undescribed function of ORF28, and may perhaps represent a novel mechanism of increasing viral replication, there are several experiments required to buttress the current data. First, protein

expression was assayed by Western blot. While some reduction in protein levels were observed, this assays for total protein levels, not surface protein levels. Given the focus on membrane proteins, further studies will necessitate the use of flow cytometry. This will provide insights into the levels of functional/correctly localized protein, instead of assaying for both surface and endocytosed protein. Next, while several promising hits were identified via proteomics, these hits were not confirmed by independent experiments and methods. Protein levels of hits need to be compared between HAORF28 and HAORF28 Δ C-term expressing cells via Western blot and flow cytometry. RT-qPCR needs to be performed to check differences in protein expression are due to post translational regulation instead of changes in transcription. Validation of these hits is required to ascertain the function of ORF28.

Additionally, HHV-8 has a broad cellular tropism and can infect a variety of cell types, including endothelial cells, B cells, monocytes, and epithelial cells. Endothelial cells are the primary targets of HHV-8 infection and are critical for the development of Kaposi's sarcoma, a type of cancer commonly associated with HHV-8 infection. HHV-8 can also infect and establish latent infection in B cells, which can lead to the development of primary effusion lymphoma and multicentric Castleman's disease.²⁴ However, these studies were done in HEK293T cells. While these cells are convenient to manipulate, they do not necessarily represent a cell type of virological interest. While the veracity of the ORF28+CHIP interaction and the hits from the proteomics is likely not impacted, some interactions and ubiquitination sites were likely not captured due to the choice to use HEK293T cells. Future studies would benefit from using a B cell line to capture proteomics more relevant to HHV-8 etiologic malignancies.

Separately, our studies focused on the role the interaction CHIP+ORF28 has on host protein levels, ignoring the other possible impacts this interaction has on CHIP functions. Under

endogenous conditions, CHIP interacts with and regulates Hsp70 and Hsp90, which in turn are molecular chaperones that plays a key role in the folding, stabilization, and activation of many client proteins. In the case of HHV-8, both Hsp 70 and Hsp90 has been shown to be important for viral replication, either due to assistance in folding and stabilization of viral proteins or activation of cellular signaling pathways that are important for replication.²⁵ Hsp90 has been shown to promote the activation of the mitogen-activated protein kinase (MAPK) pathway, which is important for the induction of the HHV-8 lytic cycle.²⁶ Inhibition of Hsp90 activity has been shown to impair KSHV replication in vitro, suggesting that the chaperone is a potential target for antiviral therapies.²⁷ Therefore, it seems possible that the alternative function of ORF28's interaction with CHIP is act as a competitive inhibitor for CHIP, freeing additional Hsp70 and Hsp90 for viral replication. This avenue was not examined, but future studies could examine the impact of a ORF28 Δ C-term mutation in a recombinant HHV-8 on replication, and see if the phenotype of the ORF28 Δ C-term virus mimics that of chemical inhibition of Hsp.

2.5 Materials and Methods

Binding assessment of CHIP to ORF28

CHIP's KD for ORF28 was determined using fluorescence polarization by measuring displacement of a fluorescent probe with a known KD (CHIP-Opt) by a non-fluorescent peptide coding for the 6 C-terminal amino acids of ORF28. FP assays were run in a black 384 well low volume plate and read on a BioTek H4 multimode plate reader at room temperature. A 4 \times stock of CHIP (21.5nM final) and a 4 \times stock of CHIPOpt Tracer (FITC-AhxLWWPD, 1nM final) was made in FP buffer (HEPES pH7.4, 50mM KCl, 0.01% TritonX-100). The 2 \times peptide dilutions were prepared in buffer (50 mM HEPES and 150 mM KCl, pH 7.4) in an 11 point serial dilution. CHIP and ORF28 peptide were mixed and incubated for 30 minutes at room temperature.

CHIPOpt tracer was added and mixed. Reads were taken at 0 minutes and 20 minutes after substrate addition. Raw polarization (mP) data were plotted relative to $\log_{10}(\text{Peptide})/M$. Data was fit to the model for $\log(\text{antagonist})$ versus response (variable slope) in Graphpad Prism 9.

Cell lines

HEK293T cells were obtained from the American Type Culture Collection (Bethesda, MD). Cells were maintained in high-glucose Dulbecco's Modified Eagle Medium (DMEM, HyClone) supplemented with 10% Fetal Bovine Serum (Gibco) and 1% penicillin/streptomycin. Cells were grown at 37°C and 5% CO₂.

Transient transfection of HEK293T cells

Constructs coding for ORF28 with an HA tag added to the N-terminus (HA-ORF28) and one where the 6 C-terminal AA coding for the CHIP binding motif were removed (HA-ORF28 Δ C-term). Constructs were transfected into HEK293T cells using TransIT293 (Mirus Bio) according to manufacturer's protocol and samples were collected for analysis 24-72 hours post transfection.

Immunocytochemistry and microscopy

HEK293T cells were plated on coverslips coated with Poly-L-Lysine and transfected as above. At 24 hours post transfection, the cells were fixed with 4% paraformaldehyde in PBS for 10 minutes, washed thrice with PBS, then permeabilized with .1% Triton in PBS. After washing the cells three times with PBST (PBS+.05% Tween20), blocking was done with 3% BSA in PBS+.05% Tween20 for one hour. Primary antibodies (HA Tag Monoclonal Antibody (2-2.2.14), #26183, Invitrogen and Anti-STUB1/CHIP Antibody, #ab134064, Abcam) were diluted 1:1000 in 3% BSA PBST overnight at 4°C. After three PBST washes, secondary was diluted 1:1000 in blocking buffer and incubated for one hour at RT before three final washes. Coverslips

were mounted using ProLong Diamond Antifade (Thermo Fisher) and imaged in the Nikon Imaging Center (University of California, San Francisco).

Immunoprecipitation

HEK293T cells were seeded and transfected as above. At 24 hours post transfection, cells were lysed and collected in IP lysis buffer (Thermo Fisher) supplemented with protease inhibitor, and spun to remove the insoluble fraction. After normalizing loading with a BCA assay, approximately 1 mg of protein lysate was used for immunoprecipitation with Pierce Anti-HA Magnetic Beads (Thermo Fisher). After an overnight incubation, samples were washed five times with IP lysis buffer, and samples eluted by incubating beads with 2x SDS-Page loading dye at 95°C for 5 minutes. Samples were then assessed via Western blot for IP and Co-IP.

Western blot

Cells were lysed in RIPA buffer or IP Lysis buffer (Thermo Fisher) supplemented with protease inhibitor, then centrifuged to remove insoluble components. Concentrations of samples were normalized using a BCA assay. Samples were run on 4-20% gradient Bis-Tris gels, and transferred to PVDF membranes using the iBLOT2 (Thermo Fisher). Membranes were blocked using 3% BSA in TBS plus .05% Tween-20 (TBST), and incubated with primary antibody overnight in the same solution at 4°C (HA Tag Monoclonal Antibody (2-2.2.14), #26183, Invitrogen; Anti-STUB1/CHIP Antibody, #ab134064, Abcam; IFNGR1 Polyclonal Antibody, #PA5-27841, Invitrogen; and Anti-HLA Class 1 ABC Antibody, #ab70328, Abcam). The membranes were washed three times with TBST, incubated with HRP-secondary diluted in the blocking buffer for 1 hour at room temperature. After three additional washes, membranes were imaged on a ChemiDoc (Biorad).

Immunoprecipitation-Mass spectrometry

HA-ORF28 overexpression samples and paired negative control (vector) samples were prepared in HEK293T cells as above, harvested by scraping, washed twice with DPBS, then IP was performed as above in a scaled up manner on 2.5 mg of total protein. Beads were flash frozen and MS sample preparation and analysis outsourced to MS-Bioworks. There, IP resin was heated for 30min in loading buffer and 50% was separated a 10% Bis-Tris Novex mini-gel (Invitrogen). The gel was stained with Coomassie and each lane was excised into ten equally sized segments and processed prior to loading for LC/MS-MS. Mascot DAT files were parsed into the Scaffold software for validation, filtering and to create a nonredundant list per sample. Data were filtered 1% protein and peptide level false discovery rate and requiring at least two unique peptides per protein. Common contaminants were removed, and threshold was set to 2-fold enrichment over vector with an unnormalized spectral count of over 4.

Ubiquitin remnant profiling

HA-ORF28 overexpression samples and paired negative control (vector) samples were prepared in HEK293T cells as above, harvested by scraping, washed twice with DPBS, and then flash frozen for processing and analysis by Creative Biosciences. Briefly, samples were resuspended in 1 mL lysis buffer (8 M urea, 1% protease inhibitor) by sonication, and insoluble fraction removed prior to assessment of protein concentration via BCA assay. 20 mg of protein per sample was diluted into 1.8 mL of lysis buffer. Disulfide bridges were reduced and reduced cysteine residues were alkylated prior to an overnight digestion at 37 °C with trypsin (Promega) using an enzyme to substrate ratio of 1:200 (w/w). TFA was added to 1% final concentration and precipitate was removed via centrifugation. Digested peptides were then purified on C18 reversed-phase columns, and the eluent was dried on a SpeedVac. Trypsin digest of proteins

leaves a di-Gly scar on ubiquitinated lysine residues, allowing for enrichment of these peptides using an antibody against this motif. The trypsin digested peptides were resuspended in IAP buffer (50 mM MOPS, pH 7.2, 10 mM sodium phosphate, 50 mM NaCl) and added K- ϵ -GG motif antibody beads. After incubation, the beads were washed with prechilled IAP buffer 4 times and HPLC grade water 4 times. The enriched peptides were eluted from the beads by 0.15% TFA and then purified by C18 column again. Samples were run on an LC-MS/MS, and raw MS files were searched against Homo sapiens protein database using Maxquant (1.6.3.4). Fold-change cutoff was set to 1.5, and significance assessed with Student's T test.

Network analysis

Enriched hits from IP-MS were used for pathway enrichment using STRING (<https://string-db.org>). Hits from ubiquitin remnant profiling were divided into upregulated and downregulated hits, and analyzed separately in STRING. Medium confidence (.4) and full STRING network was used, but text mining was excluded from analysis.

2.6 Figures and Tables

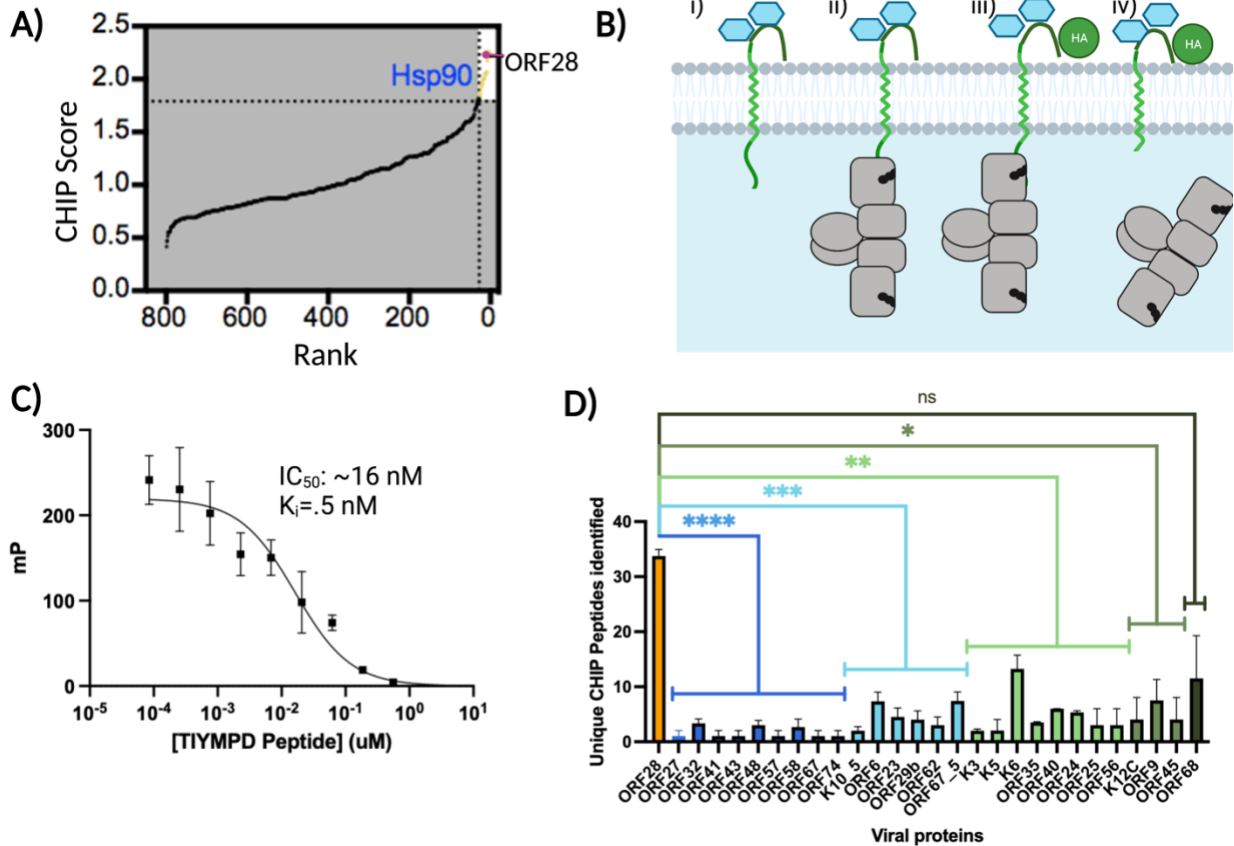


Figure 2.1: The C-terminus of ORF28 has a high affinity for CHIP.

A) Plot demonstrating likelihood of proteins from human viruses interacting with CHIP (CHIP Score) plotted against rank. Cut off CHIP Score of 1.7 (same as the canonical interactor Hsp90) was used, leading to approximately 25 viral hits. ORF28 is the top ranked hit with a CHIP Score of ~2.25. **B)** ORF28 is a small, single-pass transmembrane viral protein. The N-terminus is extracellular and glycosylated, while the C-terminus is cytoplasmically exposed (i). The exposed C-terminus is the predicted CHIP interaction site, allowing for recruitment of CHIP to the plasma membrane (ii). An HA tag was added to the N-terminus of ORF28 to enable cellular studies (HA-ORF28, iii). To determine the impact of the ORF28-CHIP interaction on ORF28 activity, the last 5 AA were removed from the C-terminus of ORF28, ablating the interaction site (HA-ORF28 Δ C-term, iv). **C)** Affinity of the ORF28 C-terminus to CHIP was determined using fluorescence polarization. CHIP has high affinity for CHIP, with a K_i of .5 nM. **D)** A previous report performed affinity purification-mass spectrometry (AP-MS) against tagged HHV-8 proteins.²⁸ ORF28 (orange) has the highest number of unique CHIP peptides associated with it out of the examined HHV-8 proteins. ORF28 has significant enrichment for CHIP peptides compared to all other HHV-8 proteins that had associated CHIP peptides except ORF28 based on ANOVA testing (**** p-value < 0.0001, *** p-value < 0.0005, ** p-value < 0.005, * p-value < 0.05, ns p-value > .05).

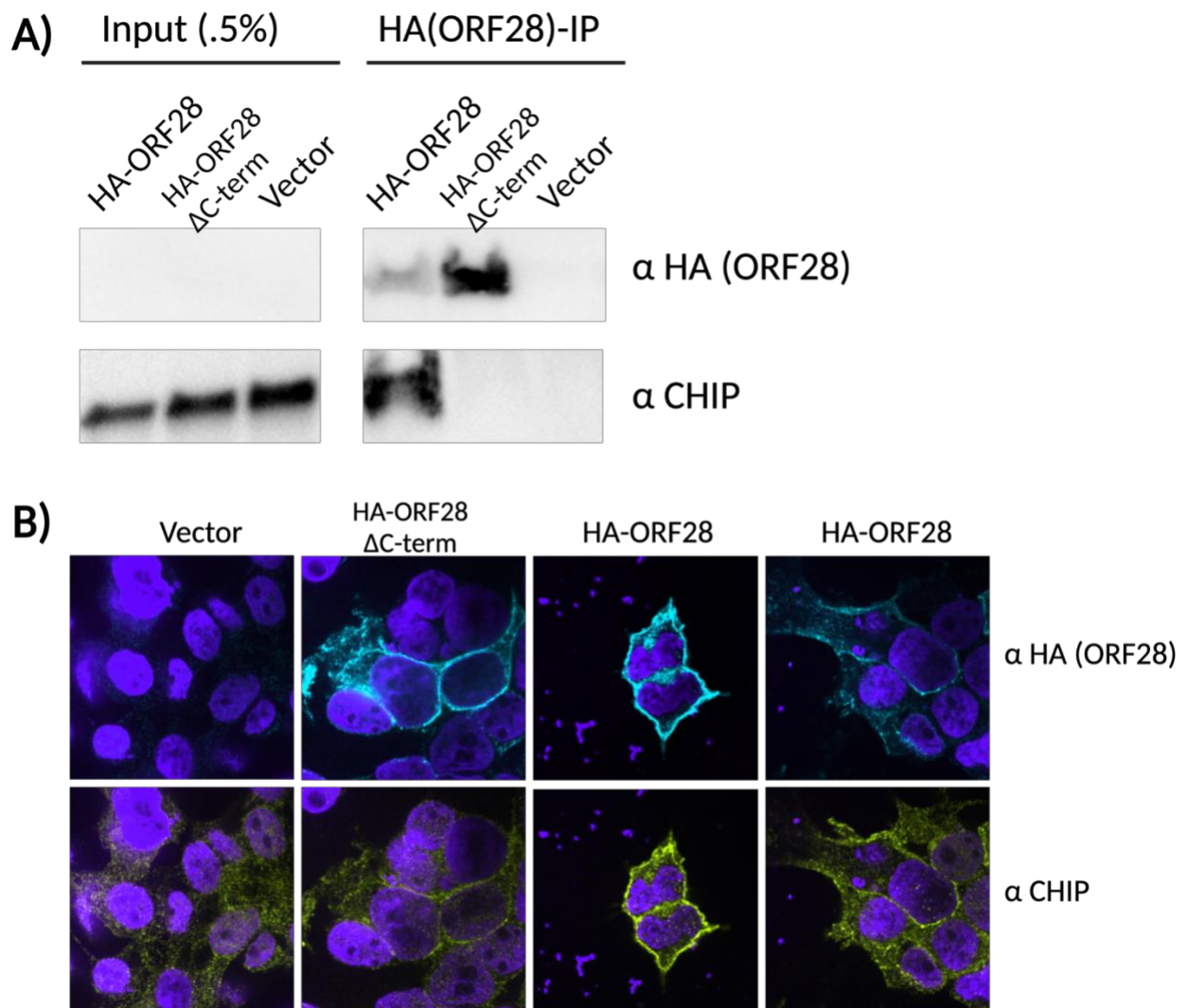


Figure 2.2: CHIP associates with HAORF28, but not HA-ORF28ΔC-term, in HEK293Ts.

A) Immunoprecipitation against the N-terminal HA tag results in successful immunoprecipitation of both HAORF28 and HAORF28ΔC-term. CHIP only coimmunoprecipitates with HAORF28, suggesting the predicted CHIP binding site on the C-terminus of ORF28 is required for the interaction. **B)** HA-tagged ORF28 localizes to the cell membrane, indicating the HA tag does not disrupt the predicted localization. CHIP is mostly cytoplasmic when HAORF28 is not expressed. HAORF28 seems to recruit CHIP to the cell membrane, matching the immunoprecipitation result. HAORF28ΔC-term has slightly more CHIP colocalization than the vector control, but less than the HAORF28.

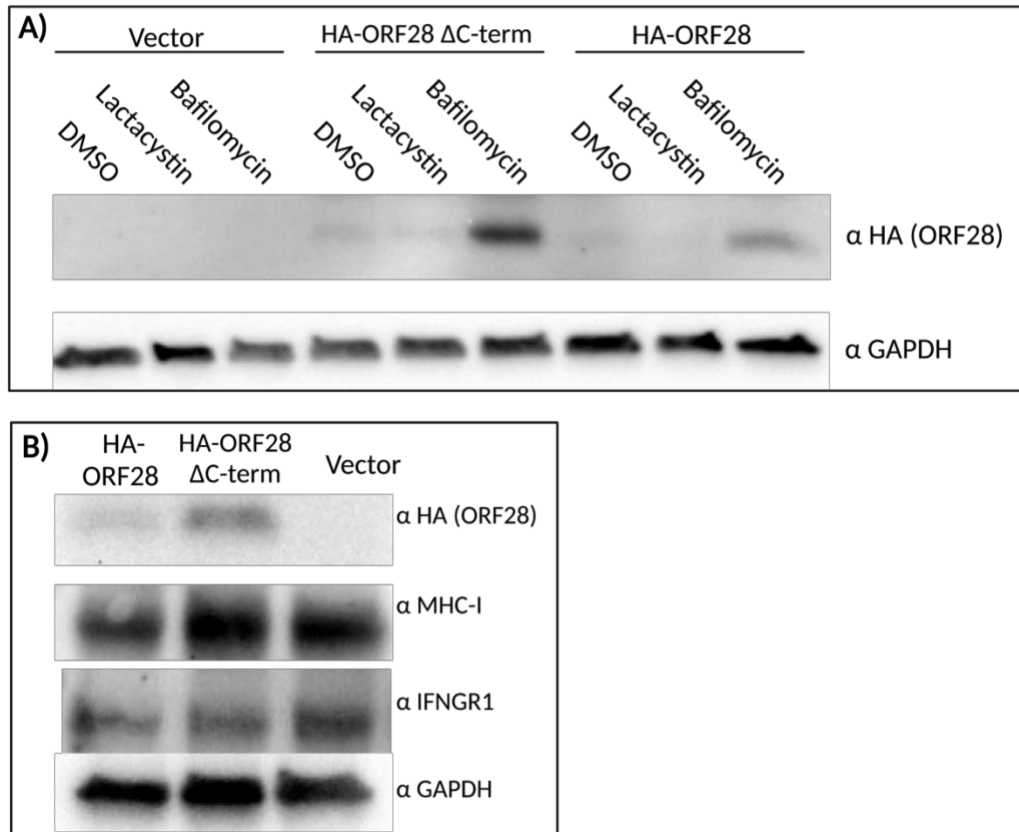


Figure 2.3: CHIP+ORF28 interaction reduces ORF28 stability and induces ubiquitination of nearby host proteins on the cell membrane.

A) HAORF28 Δ C-term has higher protein levels compared to HAORF28. Both HAORF28 and HAORF28 Δ C-term levels are increased when cells are treated with Bafilomycin (25nM), a lysosome inhibitor. Protein levels are not increased with vehicle control (DMSO) or proteasome inhibitor (Lactacystin, 10 nM). **B)** Overexpression of HAORF28 reduces total MHC-I and IFNGR1 levels compared to the vector control. HAORF28 Δ C-term expression does not impact the MHC-I expression, while reducing the IFNGR1 expression more than the vector only, less than the HAORF28.

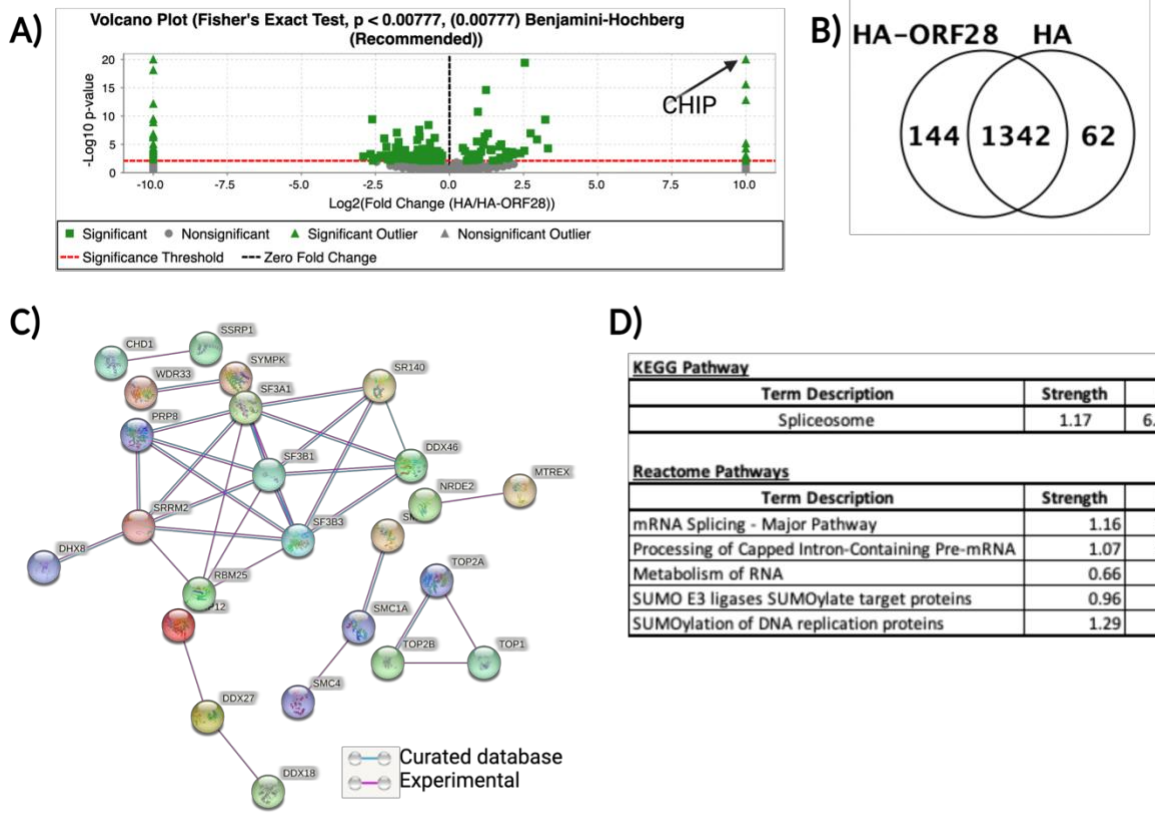


Figure 2.4: IP-MS hits enrich for mRNA processing pathways.

A) Volcano plot showing spread of enriched hits. CHIP has the highest fold enrichment and lowest p-value. **B)** Venn-diagram showing overlap in hits between the negative control (HA) and HA-ORF28 samples. 1342 proteins overlap, while 144 only appear in the HA-ORF28 samples. **C)** Hits enriched in the HA-ORF28 IP-MS show significant network enrichment. **D)** Hits enrich for pathways related to SUMOylation and mRNA splicing.

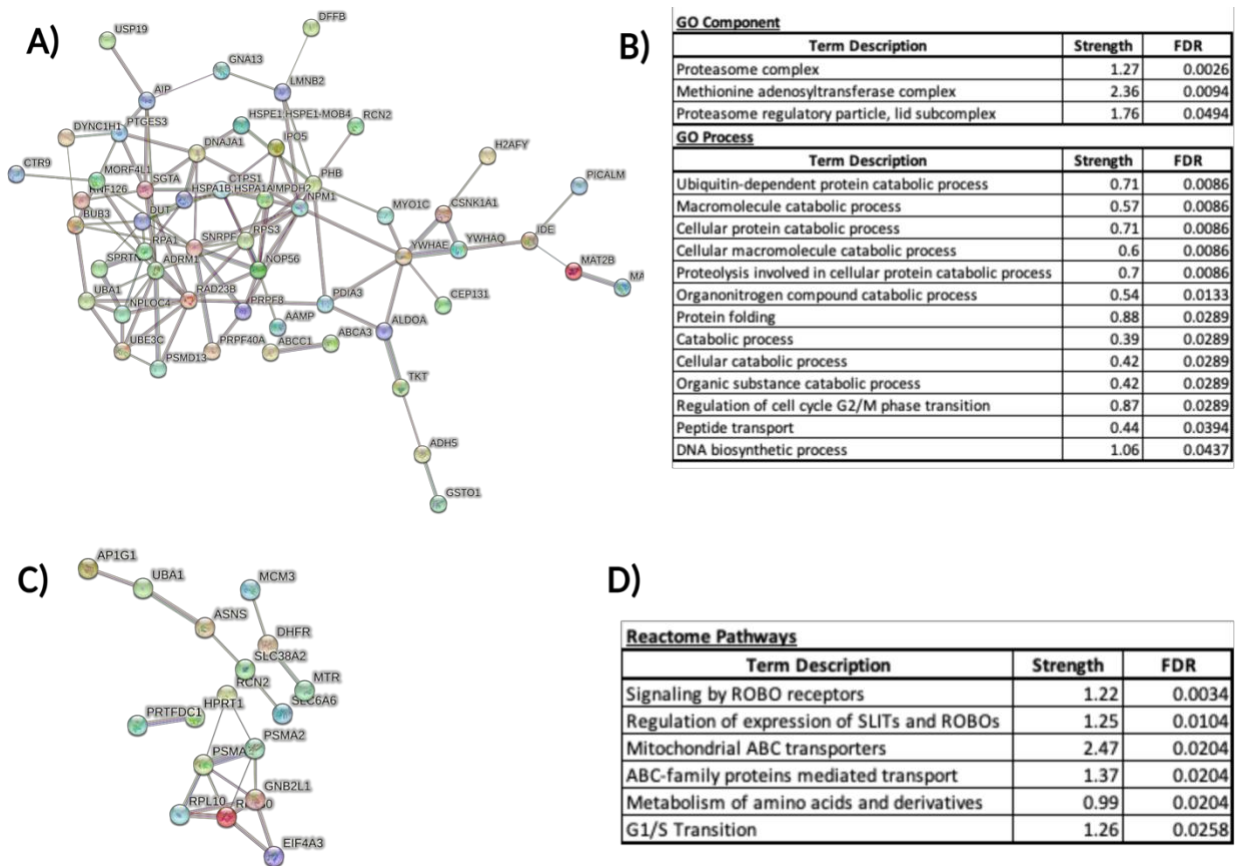


Figure 2.5: Ubiquitin remnant profiling shows increased ubiquitination of catabolism and proteasome related proteins.

A) Proteins with increased ubiquitination have significant positive network enrichment. **B)** Similar to the IP-MS enriched pathways, the proteins with increased ubiquitination are components for catabolic and proteasomal pathways. **C)** There was no significant network enrichment in the protein set with reduced ubiquitination. **D)** Proteins with decreased ubiquitination have enrichment for some pathways, but these are driven by the two ROBO proteins that showed decreased ubiquitination.

Table 2.1: IP-MS hits from HAORF28 in HEK293T cells

Accession Number	Protein	ORF28 SpC/ Control SpC	Accession Number	Protein	ORF28 SpC/ Control SpC
Q9UNE7	CHIP	NA	Q92626	PXDN	3.071
Q9BUF5	TBB6	NA	Q93008	USP9X	2.929
Q5T9A4	ATD3B	NA	Q9P035	HACD3	2.824
Q7Z3U7	MON2	NA	Q8N1F7	NUP93	2.818
Q8TER5	ARH40	NA	Q9Y5S2	MRCKB	2.800
O00443	P3C2A	NA	P60981	DEST	2.714
Q9UNZ5	L10K	NA	P10398	ARAF	2.714
Q9Y485	DMXL1	NA	P85037	FOXK1	2.667
O14795	UN13B	NA	Q9H583	HEAT1	2.636
P51610	HCFC1	NA	Q93009	UBP7	2.600
P29144	TPP2	NA	P31040	SDHA	2.600

Accession Number	Protein	ORF28 SpC/ Control SpC
Q7Z4V5	HDGR2	NA
Q16825	PTN21	NA
P21359	NF1	NA
P05386	RLA1	NA
Q9NRA8	4ET	NA
O60232	ZNRD2	NA
Q9UGJ1	GCP4	NA
Q9UPQ3	AGAP1	NA
Q92538	GBF1	NA
O60264	SMCA5	NA
Q58EX7	PKHG4	NA
O94953	KDM4B	NA
O75394	RM33	NA
Q9NP73	ALG13	NA
P02786	TFR1	NA
Q5VZE5	NAA35	NA
Q9BSJ6	PIMRE	NA
Q6ZW31	SYDE1	7.500
O14646	CHD1	6.333
Q6R327	RICTR	6.100
P02751	FINC	6.000
Q6P1N0	C2D1A	5.333
P28288	ABCD3	5.000
Q9BZF9	UACA	4.600
Q96GQ7	DDX27	4.400
Q14980	NUMA1	4.375
P11388	TOP2A	4.375
Q86VP6	CAND1	4.250
Q8N442	GUF1	4.000
P62877	RBX1	4.000
Q9HAV4	XPO5	4.000
P78332	RBM6	3.833
Q9Y4R8	TELO2	3.750
Q00610	CLH1	3.714
O14981	BTAF1	3.667
Q5JSZ5	PRC2B	3.500
Q9H4A3	WNK1	3.500
O94822	LTN1	3.429
Q81WK6	AGRA3	3.364
P07814	SYEP	3.308

Accession Number	Protein	ORF28 SpC/ Control SpC
O75179	ANR17	2.556
Q8WXA9	SREK1	2.533
Q9NXC5	MIO	2.500
Q8N5N7	RM50	2.500
P46736	BRCC3	2.500
O60841	IF2P	2.467
Q92997	DVL3	2.400
Q14151	SAFB2	2.357
P46821	MAP1B	2.333
P35606	COPB2	2.333
Q8WTT2	NOC3L	2.333
Q96S94	CCNL2	2.250
Q96A65	EXOC4	2.250
Q99755	PI51A	2.250
Q9Y5L4	TIM13	2.200
Q5XKP0	MIC13	2.200
Q01968	OCRL	2.182
Q9P015	RM15	2.167
Q9NP64	NO40	2.167
Q13009	TIAM1	2.148
Q08945	SSRP1	2.143
Q9NYU2	UGGG1	2.125
Q00325	MPCP	2.123
Q149N8	SHPRH	2.111
Q86VI3	IQGA3	2.103
Q8WVS4	DC2I1	2.087
Q5T200	ZC3HD	2.080
Q13427	PPIG	2.077
P16615	AT2A2	2.067
P27816	MAP4	2.059
Q9NTJ3	SMC4	2.040
Q92616	GCN1	2.034
O14776	TCRG1	2.026
Q2TBE0	C19L2	2.013
Q8IXB1	DJC10	2.000
Q9NVU7	SDA1	2.000
Q6P2E9	EDC4	2.000
Q6DN90	IQEC1	2.000
O95071	UBR5	2.000
O95391	SLU7	2.000

Accession Number	Protein	ORF28 SpC/ Control SpC
P49750	YLPM1	3.294
Q8N2M8	CLASR	3.286
Q8N163	CCAR2	3.250
Q13620	CUL4B	3.250
Q9Y421	FA32A	3.200

Accession Number	Protein	ORF28 SpC/ Control SpC
Q9NPA8	ENY2	2.000
Q8IX01	SUGP2	2.000
P51659	DHB4	2.000
Q9P031	TAP26	2.000
P62993	GRB2	2.000

Table 2.2: Upregulated ubiquitination sites in HEK293T cells expressing HAORF28

Accession Number	Gene Name	p-Value	Fold Change
O15269	SPTLC1	8.96E-05	2.65689
P22314	UBA1	0.00033407	5.10008
Q03252	LMNB2	0.00072459	0.78319
A0A2R8Y589	CEP78	0.00118246	1.37449
Q9NZL9	MAT2B	0.00185188	1.5249
H0YL43	RCN2	0.00187034	5.7856
P61604	HSPE1	0.00190274	3.01836
H0YAG8	ADH5	0.00226389	2.92699
Q14344	GNA13	0.00255852	4.29438
A0A1B0GV11	SLC9A6	0.00345236	0.653059
Q9Y5V3	MAGED1	0.00432962	4.20272
A0A3B3IT15	COPA	0.00491245	2.3395
K7E1Y6	RNF126	0.00520814	2.52566
P29401	TKT	0.00542994	3.39713
P54727	RAD23B	0.00719159	4.17797
P08238	HSP90AB1	0.0073855	2.75918
Q5JWB9	TMEM230	0.00790331	1.29019
M0R3F6	SUGP2	0.0087	1.32461
X6RI37	SHOC2	0.00921889	2.56155
U3KPX3	CSNK1A1	0.00959121	2.55404
O43149	ZZEF1	0.00964461	2.05588
P31689	DNAJA1	0.00965463	3.5379
Q8ND82	ZNF280C	0.0107479	0.677744
Q9UHF5	IL17B	0.0109396	6.1126
G3V2F7	UBE2V1	0.011778	3.27385
P23396	RPS3	0.0125301	1.63806
Q63HQ0	APIAR	0.0132981	1.81792
F8VUY8	SLC38A2	0.0143026	6.50715
I3L2J8	CEP131	0.0144308	3.02509
P05023	ATPIA1	0.014894	2.6532
Q8TEY7	USP33	0.0152603	2.31752
P62258	YWHAE	0.0155679	2.48715
H0YMJ0	MORF4L1	0.0155961	2.64902
P04075	ALDOA	0.016073	0.738403

Accession Number	Gene Name	p-Value	Fold Change
P27348	YWHAQ	0.022592	1.01524
J3QT28	BUB3	0.0226893	2.36389
J3QQY2	TMCO1	0.0232317	1.61754
A0A7I2V2P6	IDE	0.0232903	0.913788
P35232	PHB	0.0233081	0.969903
A0A7P0TAW9	DYNC1H1	0.0234602	1.11003
Q13492	PICALM	0.023754	3.64126
Q32Q12	NME1	0.024511	3.7232
C9JG97	AAMP	0.025816	2.11965
Q5QNY5	PEX19	0.0260861	2.32747
Q9H040	SPRTN	0.0261572	2.56153
Q9Y5V3	MAGED1	0.0262395	3.43568
H0YMP1	DUT	0.027057	2.29532
P06493	CDK1	0.0277695	0.899194
Q5TD07	NQO2	0.0281001	0.721297
P31153	MAT2A	0.0291444	0.649904
H0Y353	EDRF1	0.0298696	2.44252
A0A7I2V4T9	SGTA	0.0300509	0.665369
Q86YT6	MIB1	0.0300787	0.804764
H0Y8C6	IPO5	0.0304069	3.56728
P30101	PDIA3	0.0314858	1.64806
Q6ICB0	DESI1	0.0327171	3.6519
O75367	H2AFY	0.0336448	2.53869
H0YHD6	ASIC1	0.033821	0.635826
J3KNQ3	PSMD13	0.0341891	1.14456
H0Y3H2	ABCA3	0.0342777	1.98731
Q9NQS3	PVRL3	0.0343337	2.71044
A0A494C128	NOP56	0.0354068	3.0201
F6TX30	ASB6	0.0354778	1.9067
B4DZS0	DFFB	0.0362544	0.59495
F8VUY8	SLC38A2	0.0386429	2.68004
Q15386	UBE3C	0.0389141	1.9712
Q6PD62	CTR9	0.0399299	1.58305
E7ESU0	USP19	0.0412406	0.845032

Accession Number	Gene Name	p-Value	Fold Change
E7EQV3	PABPC1	0.0162137	3.08294
I3L4X2	ABCC1	0.0162695	3.75335
Q6P2Q9	PRPF8	0.0166233	2.11037
P40227	CCT6A	0.0172796	3.92125
H7C3C4	SLC4A7	0.0179935	2.16581
P54802	NAGLU	0.0183359	2.56595
E7ETK5	IMPDH2	0.0184132	0.838552
Q5T0S4	PPT1	0.0192002	1.40114
P41091	EIF2S3	0.0200701	3.23309
Q5TA01	GSTO1	0.0217301	3.96446
P62306	SNRPF	0.0219508	2.42307
F5H6E2	MYO1C	0.0219966	2.44095
Q15185	PTGES3	0.0223193	3.0378

Accession Number	Gene Name	p-Value	Fold Change
Q96BY2	MOAPI	0.0416113	2.11156
A0A0U1RQT8	CD99L2	0.0420499	2.94163
P0DMV9	HSPA1B	0.0425365	0.839815
Q8TAT6	NPLOC4	0.042608	0.873187
Q16186	ADRM1	0.0427344	1.87684
Q5T6Z8	TMEM59	0.0428692	3.61813
P27694	RPA1	0.0443094	1.95553
O75367	H2AFY	0.0451195	2.8492
A0A7I2V5S2	NPM1	0.0465286	3.032
A0A3B3IRI2	CTPS1	0.0467143	2.24954
A0A7N4I394	PRPF40A	0.0482923	1.4906
O75054	IGSF3	0.0491787	2.0502
O00170	AIP	0.0492312	0.952847

Table 2.3: Downregulated ubiquitination sites in HEK293T cells expressing HAORF28

Accession Number	Gene Name	p-Value	Fold Change
A0A024RA52	PSMA2	0.0381892	-0.659565
Q9NP58	ABCB7	0.0134573	-4.03217
C9JPV1	SLC6A6	0.0107242	-4.7907
A0A087WZL9	ZNF644	0.0497316	-0.708767
A0A6Q8PGM8	CHMP1A	0.0237899	-1.44069
B1ANE3	MTR	0.0458993	-2.61422
B4E1N1	ARMC6	0.0207682	-1.23708
E5RI99	RPL30	0.00098954	-3.99381
E7EN07	ACVRL1	0.00671846	-2.6266
F8VUY8	SLC38A2	0.0183103	-2.83379
F8W7C6	RPL10	0.0392153	-2.4507
F8WF48	SEC62	0.0432625	-1.8536
H0YL43	RCN2	0.00908952	-5.63278
I3L3H2	EIF4A3	0.00905766	-1.73248
Q08E86	KIAA0100	0.0449468	-1.11745
O14818	PSMA7	0.0439546	-2.3736
O43747	AP1G1	0.00537396	-1.78223
P00374	DHFR	0.0403496	-0.6442

Accession Number	Gene Name	p-Value	Fold Change
P00492	HPRT1	0.0206654	-0.705044
P08243	ASNS	0.0102072	-0.845183
P22314	UBA1	0.038164	-2.35684
P25205	MCM3	0.0396788	-0.669813
P25205	MCM3	0.0396788	-0.669813
P25205	MCM3	0.0396788	-0.669813
P28838	LAP3	0.0295727	-2.09371
P61073	CXCR4	0.0175372	-0.943419
P61073	CXCR4	0.0332487	-0.923273
P63244	GNB2L1	0.00578861	-3.62459
P63244	GNB2L1	0.0399063	-0.62546
Q5SPY9	NPDC1	0.00557632	-2.32336
Q6NSI4	CXorf57	0.0298595	-1.98011
Q7Z5G4	GOLGA7	0.0333234	-1.93497
Q96PK6	RBM14	0.0188671	-1.07152
Q96PK6	RBM14	0.00629394	-3.14274
Q9NQX4	MYO5C	0.0178709	-0.900265
Q9UNY4	TTF2	0.0182864	-0.611749

2.7 References

- (1) Lin, H.-C.; Yeh, C.-W.; Chen, Y.-F.; Lee, T.-T.; Hsieh, P.-Y.; Rusnac, D. V.; Lin, S.-Y.; Elledge, S. J.; Zheng, N.; Yen, H.-C. S. C-Terminal End-Directed Protein Elimination by CRL2 Ubiquitin Ligases. *Molecular Cell* **2018**, *70* (4), 602-613.e3.
<https://doi.org/10.1016/j.molcel.2018.04.006>.
- (2) Koren, I.; Timms, R. T.; Kula, T.; Xu, Q.; Li, M. Z.; Elledge, S. J. The Eukaryotic Proteome Is Shaped by E3 Ubiquitin Ligases Targeting C-Terminal Degrons. *Cell* **2018**, *173* (7), 1622-1635.e14. <https://doi.org/10.1016/j.cell.2018.04.028>.
- (3) Ravalin, M.; Basu, K.; Gestwicki, J. E.; Craik, C. S. End-Binding E3 Ubiquitin Ligases Enable Protease Signaling. *ACS Chem. Biol.* **2019**, *acschembio.9b00621*.
<https://doi.org/10.1021/acschembio.9b00621>.
- (4) Ravalin, M.; Theofilas, P.; Basu, K.; Opoku-Nsiah, K. A.; Assimon, V. A.; Medina-Cleghorn, D.; Chen, Y.-F.; Bohn, M. F.; Arkin, M.; Grinberg, L. T.; Craik, C. S.; Gestwicki, J. E. Specificity for Latent C Termini Links the E3 Ubiquitin Ligase CHIP to Caspases. *Nat Chem Biol* **2019**, *15* (8), 786–794. <https://doi.org/10.1038/s41589-019-0322-6>.
- (5) Murata, S.; Minami, Y.; Minami, M.; Chiba, T.; Tanaka, K. CHIP Is a Chaperone-Dependent E3 Ligase That Ubiquitylates Unfolded Protein. *EMBO Rep.* **2001**, *2* (12), 1133–1138.
<https://doi.org/10.1093/embo-reports/kve246>.
- (6) Qian, S.-B.; McDonough, H.; Boellmann, F.; Cyr, D. M.; Patterson, C. CHIP-Mediated Stress Recovery by Sequential Ubiquitination of Substrates and Hsp70. *Nature* **2006**, *440* (7083), 551–555. <https://doi.org/10.1038/nature04600>.

- (7) Ali, A.; Kumar, V.; Banerjea, A. C. STUB1/CHIP Promotes Ubiquitination and Degradation of HIV-1 Vif to Restore the Cellular Level of APOBEC3G Protein. *Biochemical and Biophysical Research Communications* **2021**, *574*, 27–32.
<https://doi.org/10.1016/j.bbrc.2021.08.031>.
- (8) Lin, J.; Yin, L.; Xu, X.-Z.; Sun, H.-C.; Huang, Z.-H.; Ni, X.-Y.; Chen, Y.; Lin, X. Bay41-4109-Induced Aberrant Polymers of Hepatitis b Capsid Proteins Are Removed via STUB1-Promoted P62-Mediated Macroautophagy. *PLoS Pathog* **2022**, *18* (1), e1010204.
<https://doi.org/10.1371/journal.ppat.1010204>.
- (9) Arias, C.; Weisburd, B.; Stern-Ginossar, N.; Mercier, A.; Madrid, A. S.; Bellare, P.; Holdorf, M.; Weissman, J. S.; Ganem, D. KSHV 2.0: A Comprehensive Annotation of the Kaposi's Sarcoma-Associated Herpesvirus Genome Using Next-Generation Sequencing Reveals Novel Genomic and Functional Features. *PLoS Pathog* **2014**, *10* (1), e1003847.
<https://doi.org/10.1371/journal.ppat.1003847>.
- (10) May, J. S.; Coleman, H. M.; Boname, J. M.; Stevenson, P. G. Murine Gammaherpesvirus-68 ORF28 Encodes a Non-Essential Virion Glycoprotein. *Journal of General Virology* **2005**, *86* (4), 919–928. <https://doi.org/10.1099/vir.0.80661-0>.
- (11) TerBush, A. A. Characterization of Receptor Use and Entry Mechanisms in Two KSHV Infection Systems. PhD, UC Berkeley, 2018.
- (12) Gram, A. M.; Oosenbrug, T.; Lindenbergh, M. F. S.; Büll, C.; Comvalius, A.; Dickson, K. J. I.; Wiegant, J.; Vrolijk, H.; Lebbink, R. J.; Wolterbeek, R.; Adema, G. J.; Griffioen, M.; Heemskerk, M. H. M.; Tschärke, D. C.; Hutt-Fletcher, L. M.; Wiertz, E. J. H. J.; Hoeben, R. C.; Rensing, M. E. The Epstein-Barr Virus Glycoprotein Gp150 Forms an Immune-

- Evasive Glycan Shield at the Surface of Infected Cells. *PLoS Pathog* **2016**, *12* (4), e1005550. <https://doi.org/10.1371/journal.ppat.1005550>.
- (13) Coscoy, L.; Ganem, D. Kaposi's Sarcoma-Associated Herpesvirus Encodes Two Proteins That Block Cell Surface Display of MHC Class I Chains by Enhancing Their Endocytosis. *Proceedings of the National Academy of Sciences* **2000**, *97* (14), 8051–8056. <https://doi.org/10.1073/pnas.140129797>.
- (14) Brulois, K.; Toth, Z.; Wong, L.-Y.; Feng, P.; Gao, S.-J.; Ensser, A.; Jung, J. U. Kaposi's Sarcoma-Associated Herpesvirus K3 and K5 Ubiquitin E3 Ligases Have Stage-Specific Immune Evasion Roles during Lytic Replication. *Journal of Virology* **2014**, *88* (16), 9335–9349. <https://doi.org/10.1128/JVI.00873-14>.
- (15) Kopp, Y.; Lang, W.-H.; Schuster, T. B.; Martínez-Limón, A.; Hofbauer, H. F.; Ernst, R.; Calloni, G.; Vabulas, R. M. CHIP as a Membrane-Shuttling Proteostasis Sensor. *eLife* **2017**, *6*, e29388. <https://doi.org/10.7554/eLife.29388>.
- (16) Rezaee, S. A. R. Kaposi's Sarcoma-Associated Herpesvirus Immune Modulation: An Overview. *Journal of General Virology* **2006**, *87* (7), 1781–1804. <https://doi.org/10.1099/vir.0.81919-0>.
- (17) Okiyoneda, T.; Barriere, H.; Bagdany, M.; Rabeh, W. M.; Du, K.; Hohfeld, J.; Young, J. C.; Lukacs, G. L. Peripheral Protein Quality Control Removes Unfolded CFTR from the Plasma Membrane. *Science* **2010**, *329* (5993), 805–810. <https://doi.org/10.1126/science.1191542>.
- (18) Koochaki, S. H. J.; Słabicki, M.; Lumpkin, R.; Zou, C.; Belizaire, R.; Fischer, E. S.; Ebert, B. L. A STUB1 Ubiquitin Ligase/CHIC2 Protein Complex Negatively Regulates the IL-3, IL-5, and GM-CSF Cytokine Receptor Common β Chain (CSF2RB) Protein Stability.

Journal of Biological Chemistry **2022**, 298 (10), 102484.

<https://doi.org/10.1016/j.jbc.2022.102484>.

- (19) Apriamashvili, G.; Vredevoogd, D. W.; Krijgsman, O.; Bleijerveld, O. B.; Ligtenberg, M. A.; de Bruijn, B.; Boshuizen, J.; Traets, J. J. H.; D'Empaire Altimari, D.; van Vliet, A.; Lin, C.-P.; Visser, N. L.; Londino, J. D.; Sanchez-Hodge, R.; Oswalt, L. E.; Altinok, S.; Schisler, J. C.; Altelaar, M.; Peeper, D. S. Ubiquitin Ligase STUB1 Destabilizes IFN γ -Receptor Complex to Suppress Tumor IFN γ Signaling. *Nat Commun* **2022**, 13 (1), 1923. <https://doi.org/10.1038/s41467-022-29442-x>.
- (20) Ng, S.; Lim, S.; Sim, A. C. N.; Mangadu, R.; Lau, A.; Zhang, C.; Martinez, S. B.; Chandramohan, A.; Lim, U.-M.; Ho, S. S. W.; Chang, S. C.; Gopal, P.; Hong, L. Z.; Schwaid, A.; Fernandis, A. Z.; Loboda, A.; Li, C.; Phan, U.; Henry, B.; Partridge, A. W. STUB1 Is an Intracellular Checkpoint for Interferon Gamma Sensing. *Sci Rep* **2022**, 12 (1), 14087. <https://doi.org/10.1038/s41598-022-18404-4>.
- (21) Cai, Q.; Cai, S.; Zhu, C.; Verma, S. C.; Choi, J.-Y.; Robertson, E. S. A Unique SUMO-2-Interacting Motif within LANA Is Essential for KSHV Latency. *PLoS Pathog* **2013**, 9 (11), e1003750. <https://doi.org/10.1371/journal.ppat.1003750>.
- (22) Campbell, M.; Izumiya, Y. Post-Translational Modifications of Kaposi's Sarcoma-Associated Herpesvirus Regulatory Proteins – SUMO and KSHV. *Front. Microbio.* **2012**, 3. <https://doi.org/10.3389/fmicb.2012.00031>.
- (23) Majerciak, V.; Yamanegi, K.; Allemand, E.; Kruhlik, M.; Krainer, A. R.; Zheng, Z.-M. Kaposi's Sarcoma-Associated Herpesvirus ORF57 Functions as a Viral Splicing Factor and Promotes Expression of Intron-Containing Viral Lytic Genes in Spliceosome-Mediated RNA Splicing. *J Virol* **2008**, 82 (6), 2792–2801. <https://doi.org/10.1128/JVI.01856-07>.

- (24) Sunil, M.; Reid, E.; Lechowicz, M. J. Update on HHV-8-Associated Malignancies. *Curr Infect Dis Rep* **2010**, *12* (2), 147–154. <https://doi.org/10.1007/s11908-010-0092-5>.
- (25) Baquero-Pérez, B.; Whitehouse, A. Hsp70 Isoforms Are Essential for the Formation of Kaposi's Sarcoma-Associated Herpesvirus Replication and Transcription Compartments. *PLoS Pathogens* **2015**, *11* (11), e1005274. <https://doi.org/10.1371/journal.ppat.1005274>.
- (26) Wen, K. W.; Damania, B. Hsp90 and Hsp40/Erdj3 Are Required for the Expression and Anti-Apoptotic Function of KSHV K1. *Oncogene* **2010**, *29* (24), 3532–3544. <https://doi.org/10.1038/onc.2010.124>.
- (27) Chen, W.; Sin, S.-H.; Wen, K. W.; Damania, B.; Dittmer, D. P. Hsp90 Inhibitors Are Efficacious against Kaposi Sarcoma by Enhancing the Degradation of the Essential Viral Gene LANA, of the Viral Co-Receptor EphA2 as Well as Other Client Proteins. *PLoS Pathog* **2012**, *8* (11), e1003048. <https://doi.org/10.1371/journal.ppat.1003048>.
- (28) Davis, Z. H.; Verschueren, E.; Jang, G. M.; Kleffman, K.; Johnson, J. R.; Park, J.; Von Dollen, J.; Maher, M. C.; Johnson, T.; Newton, W.; Jäger, S.; Shales, M.; Horner, J.; Hernandez, R. D.; Krogan, N. J.; Glaunsinger, B. A. Global Mapping of Herpesvirus-Host Protein Complexes Reveals a Transcription Strategy for Late Genes. *Molecular Cell* **2015**, *57* (2), 349–360. <https://doi.org/10.1016/j.molcel.2014.11.026>.

Chapter 3: Generation of a SARS-CoV-2 RNA Replicon for Antiviral Drug Screening

3.1 Abstract

Antiviral screening efforts and virology studies for severe acute respiratory syndrome coronavirus 2 (SARS-CoV-2) are limited by the availability of biosafety level (BSL) 3 lab space to perform live virus assays. Stable replicon lines can act as models of viral replication, without recapitulating viral entry and egress due to removal of structural proteins. The spike (S) gene was replaced with a reporter-resistance fusion protein, and the envelope (E) and membrane (M) genes were removed from the viral genome. By omitting the entry and egress portion of the SARS-CoV-2 lifecycle, these cell lines can model replication without the formation of infectious virions, allowing for BSL-2 containment. While low levels of replication and reporter activity were observed months after initial transfection of replicon RNA template, replication levels were not high enough for most virology studies or antiviral screening campaigns.

3.2 Introduction

SARS-CoV-2, the etiologic agent of COVID-19, was first described in Wuhan, China in late 2019.¹ The pathogenicity and infectivity of SARS-CoV-2 underscores the need for the development of vaccines and antivirals, as well as further elucidation of the viral life cycle. Traditional methods of measuring antiviral activity are often low throughput, and, in the case of SARS-CoV-2, need to be performed at BSL-3. Screening throughput for antivirals can be increased by incorporating reporters into viral genomes via reverse genetics and the generation of replicons.^{2,3} Coronavirus reverse genetics systems are technically challenging due to the large size of the viral genome (approximately 30kb), and sections of viral genomes inhibiting bacterial growth.² These problems can be circumvented using bacterial artificial chromosomes, vaccinia virus, and *in vitro* ligation of cDNA fragments.^{2,4-6} These approaches were quickly applied to SARS-CoV-2, and multiple studies demonstrated reverse genetics systems using *in vitro* ligation

of cDNA fragments and a novel yeast genetics platform to successfully generate infectious virions.⁷⁻⁹ However, these systems still require BSL-3 containment, rendering them of limited utility to many labs.

To address this, multiple groups attempted to generate replicons. SARS-CoV-2 replicons can be used to study the mechanisms of viral replication and test the efficacy of antiviral drugs in a BSL-2 setting, which is much more accessible to the research community. These modified genomes are engineered to contain the genes required for RNA replication and deleting the genes responsible for virus assembly and packaging. The RNA molecules are introduced into cells where they can replicate, allowing researchers to study the viral RNA replication cycle without the need for a fully infectious virus.

However, SARS-CoV-2 replicons proved harder to generate than the reverse genetics systems. Most early iterations were unwieldy and only provided transient replication.¹⁰⁻¹³ To address this, we attempted to create and characterize stably replicating SARS-CoV-2 replicon cell lines. This chapter describes our efforts to generate a SARS-CoV-2 replicon based on a previously reported severe acute respiratory syndrome (SARS) replicon.⁶ Briefly, the structural genes S, E, and M were removed, precluding the formation of infectious virions. A reporter-resistance marker fusion gene replaced S, allowing for selection of replicon bearing cells. We anticipated these cells could be used for replication studies, as well as screening of antivirals. However, these cells were unable to support adequate levels of replication for antiviral screening, and a publication indicates sufficient replication levels may require the introduction of mutations into non-structural protein 1 (Nsp1).¹⁴

3.3 Results

Replicon RNA generation, transfection, and selection of stable cell lines

DNA template for *in vitro* transcription of SARS-CoV-2 replicon RNA was generated using similar approaches to those described for SARS-CoV-2 reverse genetics systems using ligation of cDNA fragments.^{7,8} Full-length template was generated in a multi-step process (**Figure 3.1a**). Two reporters (NLuc and GFP) fused to the Blasticidin resistance protein (BSD) and two combinations of viral accessory proteins (inclusion or exclusion of ORFs 6-8) were tested, leading to four templates for initial attempts at establishing replicons (**Figure 3.1b**). While there were contaminating incomplete products in the ligation mixtures, full-length product was visible in the diagnostic agarose gel (**Figure 3.1c**). Ligations were purified in bulk with the contaminating products, as gel extraction of the correct band size resulted in yield losses too significant for progression to transcription. *In vitro* transcription generated a smear of products, an expected result given the length (~25 kb) of the replicon template (**Figure 3.1d**). After a DNase digestion to remove the DNA template, the RNA products were purified and then introduced to a variety of cell lines known to support viral replication in infections and replicons. Initial efforts involved both transfection and electroporation of replicon RNA into VeroE6, HeLa, BHK-21, HEK293, A549, Huh7, and Huh7.3.1 cell lines. This attempt did not yield successful production of reporter. Subsequent attempts included N RNA in the mixture, as other reports indicate N protein assists in replication.¹⁵ After multiple weeks of selections, clones arose in VeroE6 cells transfected with the GFPL (includes ORF 6-8) and GFPS (excludes ORF 6-8) RNA. These cells were blasticidin resistant and expressed (**Figure 3.1e**). These clones were expanded, banked, and tested for replication. Despite multiple attempts, we were unable to generate blasticidin resistant clones with the NLuc+BSD reporter.

Vero replicon clones produce viral proteins and show evidence of genome replication

To determine if the clones had replicon RNA and were replicating the modified viral genome, we examined the clones for protein expression, RNA levels, and checked for integration of contaminating template DNA. Via immunofluorescence these cells were positive for dsRNA, which is a marker of viral replication, as the viral lifecycle requires synthesis of a negative strand of the RNA genome to produce additional genome copies. Also via immunofluorescence, multiple clones were positive for viral proteins the viral proteins N and major protease (M^{Pro}) (**Figure 3.2a**). These clones were also positive for N protein via Western blot (**Figure 3.2b**).

Protein expression correlated to RNA levels based on RT-PCR. Additionally, RNA levels of BSD were higher than those of ORF1A/ORF1B. This is expected as the GFP-BSD fusion protein expression is driven off the S transcriptional start site, leading to higher transcription levels than that of ORF1A/B (**Figure 3.2c**). These clones do not have detectable levels of integrated template DNA in the cell genomes, indicating RNA transcripts and protein expression are being driven by replicon replication (**Figure 3.2d**). These data suggest the clones have stable replicon genomes, as these experiments were performed over a month and multiple passages after transfection, meaning the original RNA replicon genomes would have degraded or diluted out by the time these experiments were performed.

Replicon cells do not produce sufficient reporter levels for compound screening

These clones were then tested for reporter response to known SARS-CoV-2 replication inhibitors. After five days of treatment with GC376, an M^{Pro} inhibitor with broad reactivity across several viral proteases, both GFPS and GFPL showed a reduction in percentage of GFP positive cells at two doses when compared to a DMSO control (**Figure 3.3a**). However, the drop in GFP positivity was only 5-15% of the total cell population, and only 20-40% of the GFP

positive population after normalizing to the DMSO negative control (**Figure 3.3b**). Separately, cells were treated for five days with remdesivir, a known RNA-dependent RNA polymerase (RDRP) inhibitor. Both tested replicon lines had no to minimal response to remdesivir treatment, although it is uncertain if the poor response was due to inactive compound or poor cellular response to the inhibitor (**Figure 3.3b and c**). GFPS C2 had overall better responses to the inhibitors but did not respond well enough to recapitulate published EC50 values for both inhibitors from the literature (**Figure 3.3c**).

3.4 Discussion

A stable replicon's utility is especially valuable in the identification of new and repurposed inhibitors, an existing bottleneck slowing many SARS-CoV-2 replication inhibitor discovery efforts. To enable high-throughput compound screening and replication studies in a BSL 2 environment, we worked to develop reporter replicon lines with fluorescent or luminescent markers to use as surrogates for viral replication. This would allow for high-throughput, plate-based inhibitor screens, as well as enabling flow cytometry-based replication studies. However, the described design iterations were unsuitable for inhibitor screening and replication studies due to insufficient reporter levels for acceptable assay windows.

Inadequate reporter levels seem to be driven by a combination of poor replication, and only a small subpopulation of cells harboring detectable levels of reporter. We attempted to raise reporter levels by increasing stringency of antibiotic selections, as well as designing replicons with the reporter under different transcriptional start sites (**Supplementary Figure 3.1**). Increased antibiotic concentrations briefly raised reporter levels, but cells were unable to sustain the increased replication over longer periods of time. Via immunofluorescence, fluorescent cell counting, and flow cytometry, only around 5-30% of each clonal cell line maintained detectable

replication. We attempted to sort for and expand GFP positive populations but found that the sorted cells shifted from 100% GFP positive back to the original percentage positive within a few passages (data not shown). This seems to indicate a need for adaptive mutations in the replicon or further adjustment in the design. In fact, the only published stable SARS-CoV-2 replicon showed a requirement for two mutations in the Nsp 1.¹⁴

The next avenue attempted to increase percentage of reporter positive cells and overall reporter levels was to change the reporter to a GFP-ZeoR or ZeoR-GFP fusion protein and incorporate the afore mentioned Nsp 1 mutations. Placing the new GFP-ZeoR reporter under an IRES in ORF1A or under the S transcriptional start site increased reporter levels and proportions of GFP-positive cells and resulted in colony formation in a shorter time compared the GFP-BSD cell lines. This is presumably due to the difference in mechanism between the ZeoR and BSD, where ZeoR inhibits antibiotic function by directly binding to the Zeocin, while BSD functions enzymatically. These GFP-ZeoR cells were frozen and banked. We next planned to expand these clones, increase selection pressure to further drive up the proportion of GFP positive cells/reporter levels, and then assay for reporter response to GC376 and remdesivir. If these cells had a superior response to the inhibitors compared to the BSD lines, we intended to examine viral protein expression, sequence the replicon genomes to look for adaptive mutations, and perform resistance studies to include in a publication.

3.5 Materials and Methods

Cell lines

Baby Hamster Kidney cells (BHK-21, CCL10) and HEK293T cells were obtained from the American Type Culture Collection (Bethesda, MD). African green monkey kidney epithelial cells (Vero E6) and human lung epithelial-like cells (A549) were a generous gift from Nevan

Krogan's lab (University of California, San Francisco). Human hepatocellular carcinoma lines (Huh7 and Huh7.3.1) and human cervical adenocarcinoma cells (HeLa) were generous gifts from Andreas Puschnik's group (Chan Zuckerberg Biohub). All cells were maintained in high-glucose Dulbecco's Modified Eagle Medium (DMEM, HyClone) with 10% Fetal Bovine Serum (Gibco) and 1% penicillin/streptomycin. Cells were grown at 37°C and 5% CO₂.

Assembly of full-length SARS-CoV-2 replicon cDNA template

Replicon designs were based on a previously described Severe Acute Respiratory Syndrome (SARS) replicon for drug discovery and a virus strain (GenBank Accession: MN908947) from Wuhan^{46,51}. Six silent mutations were introduced to remove endogenous BsaI and BsmBI sites from the viral genome to facilitate downstream molecular biology. cDNAs were synthesized and cloned into the pTwistAmpMed plasmid by Twist Biosciences. These cDNAs were not suitable for direct digestion and ligation due to plasmid instability in *E. coli*. Instead, the cDNAs were used as PCR templates and amplified by Q5 High-Fidelity DNA Polymerase (New England Biolabs). BsaI sites were included at the end of each of the six fragments for scarless assembly. Each fragment was individually digested overnight with BsaI and purified using NucleoSpin Gel and PCR Clean-up (Machery-Nagel). Ligation of the 6 fragments simultaneously and sequentially did not yield sufficient full-length replicon DNA template to proceed with transcription. To generate reagent quantities of full-length replicon template DNA, equimolar amounts of fragments 1-2 and 3-6 were separately ligated overnight at 16°C using T4 ligase (New England Biolabs). These ligations were used as PCR templates and amplified using Q5 to generate large quantities of fragments 1-2 and 3-6. These fragments were extracted from .6% agarose gels using the NucleoSpin Gel and PCR Clean-up kit, BsaI digested overnight, and purified again. Equimolar amounts of fragments 1-2 and 3-6 were ligated together overnight at

16°C using T4 ligase, generating the full-length replicon template. The resulting ligation was purified by phenol/chloroform extraction and isopropanol precipitation.

RNA transcription, transfection, and selection of stable replicon lines

.5 to 1 ug of purified ligation were used as template for *in vitro* transcriptions. RNA transcripts were generated using HiScribe T7 ARCA mRNA kit with tailing (New England Biolabs) reaction with a two-hour incubation time and a reaction scaled to 50 ul. DNA template was removed and the resulting RNA polyadenylated following the manufacturer's protocol. The RNA was purified according to New England Biolab's guidelines by LiCl precipitation and washed with 70% ethanol. The air-dried pellet was dissolved in 30 uL of RNase-free water.

Transfection of cells

Cells were seeded one day prior to transfection at densities of 250k-500k cells per 6 well. The following day, they were transfected with .5-3ug of RNA using MessengerMax (Thermo Scientific) according to manufacturer's instructions.

Selections

24 hours post transfection, selections were started using the appropriate antibiotics. Concentrations were adjusted according to cell line and growth (50-500 ug/mL for blasticidin, .5-10 ug/mL for zeocin).

Immunofluorescence

Cells bearing replicons and matched untransfected cells were plated on coverslips coated with Poly-L-Lysine. At 24 hours post plating, they were fixed for 10 minutes using 4% paraformaldehyde in PBS, washed thrice with PBS, then permeabilized with .1% Triton in PBS. After washing the cells three times with PBST (PBS+.05% Tween20), blocking was done with 3% BSA in PBS+.05% Tween20 for one hour. Primary antibodies (SARS-CoV-2 Nucleocapsid

Protein Antibody #33336, Cell Signaling Technology and Anti-dsRNA Antibody, clone rJ2 #MABE1134, Sigma Aldrich) were diluted 1:1000 in 3% BSA PBST overnight at 4°C. After three PBST washes, secondary was diluted 1:1000 in blocking buffer and incubated for one hour at RT before three washes. Coverslips were mounted using ProLong Diamond Antifade (Thermo Fisher) and imaged in the Nikon Imaging Center (University of California, San Francisco).

Western blot

Cells were lysed in RIPA buffer supplemented with protease inhibitor, then centrifuged to remove insoluble components. Concentrations of samples were normalized using a BCA assay. Samples were run on 4-20% gradient Bis-Tris gels, and transferred to PVDF membranes using the iBLOT2 (Thermo Fisher). Membranes were blocked using 3% BSA in TBST, and incubated with primary antibody overnight in the same solution at 4°C (SARS-CoV-2 Nucleocapsid Protein Antibody #33336, Cell Signaling Technology, Beta-Actin Antibody #A5316, Sigma Aldrich). The membranes were washed three times with TBST, incubated with HRP-secondary diluted in the blocking buffer for 1 hour at room temperature, washed three more times, and then imaged on a BioRad ChemiDoc.

RT-PCR and genomic DNA PCR

Replicon RNAs were extracted from 1×10^6 cells following the manufacturer's protocol with TRIzol Reagent (Thermo Fisher Scientific) and resuspended in 60 ul of water. These samples were reverse transcribed with SuperScript III First-Strand Synthesis System (Thermo Fisher Scientific) or qScript XLT 1-Step RT-PCR Kit using SARS-CoV-2 specific primers. To examine genomic integration of contaminating template DNA, genomic DNA was extracted using QIAamp DNA mini kit (Qiagen). Purified DNA was used as a PCR template to assess for the presence of nucleocapsid or BSD DNA in samples.

Reporter response to compound treatment

Replicon-bearing cells in DMEM+5% FBS+P/S+2.5ug/mL Blasticidin were plated at 200,000 cells/well in 6 well plates. GC376 and remdesivir (MedChem Express) were diluted in DMSO to generate 200x stock solutions, then diluted 1:200 in DMEM+5% FBS+P/S+2.5ug/mL Blasticidin. One day post plating, the media was replaced with compound containing media. After four days of treatment, the cells were removed from the well using trypsin, washed, and run on a FACS Aria II to assess fluorescence. Data were analyzed in FlowJo.

3.6 Figures

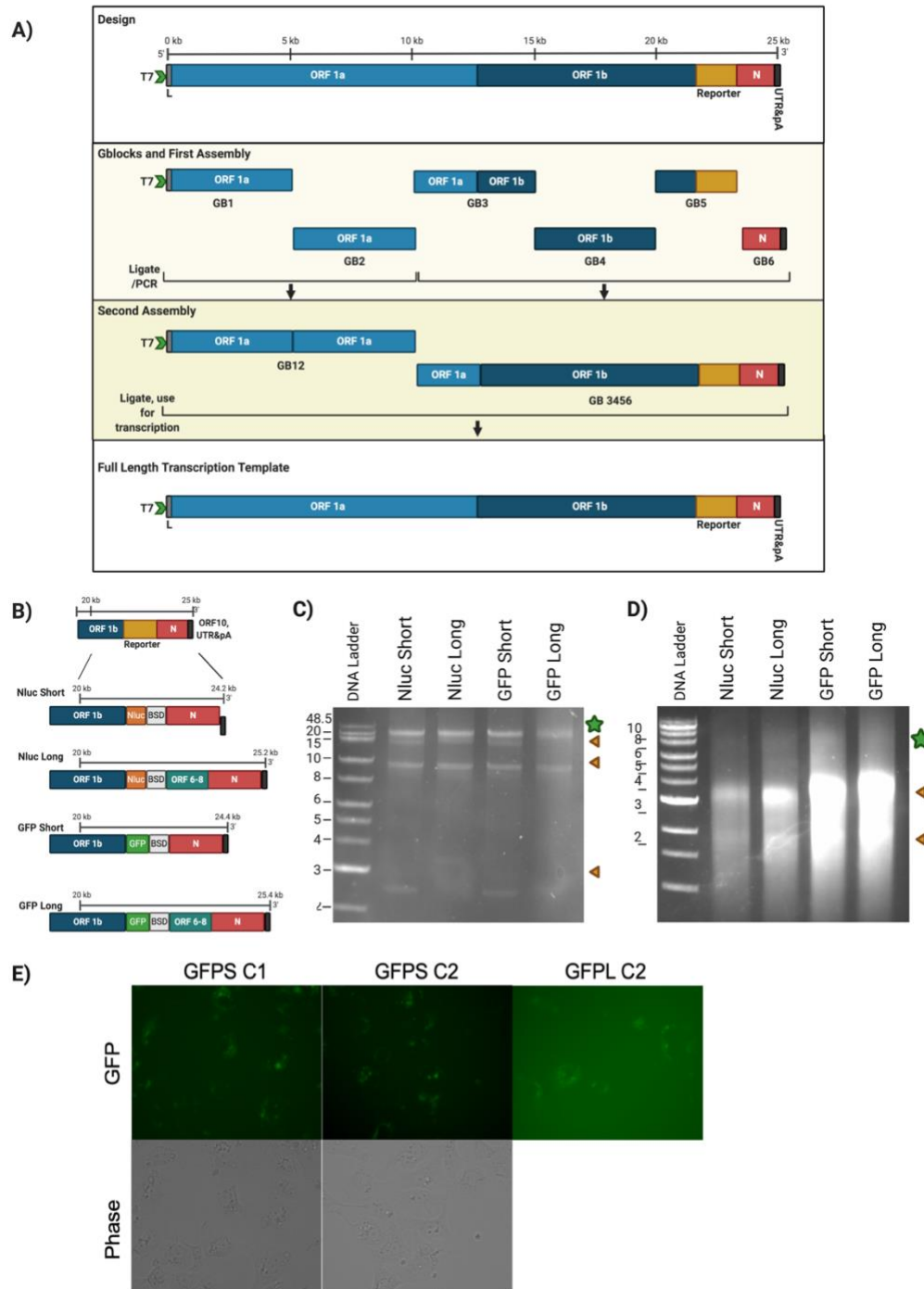


Figure 3.1: Overview of SARS-CoV-2 replicons tested

A) The replicon design removed genes M and E, and replaced S with a reporter-blasticidin resistance (BSD) gene. Five gene fragments spanning the entire design were synthesized. Full-length transcriptional templates were assembled in two sequential rounds of PCR, digestion and ligation. **B)** Four different replicon designs were initially attempted. Designs used one of two reporters (Nluc-BSD or GFP-BSD).

The long (L) designs include all ORFs after ORF6, while the short (S) designs only included nucleocapsid. Additional tested designs are annotated in **Supplementary Figure 3.1**. **C**) Representative DNA gel (.7% non-denaturing agarose) showed full-length assembly of transcription templates for each construct. Full-length template is designated with green star, while incomplete products are designated with a triangle. **D**) Non-denaturing gel (.7% agarose) of *in vitro* transcribed RNA. Presumed full length replicon RNA is designated with green star, while incomplete products are designated with a triangle. **E**) After introducing the replicon RNA into cells via transfection, cells bearing replicons were selected using blasticidin. At one month of selection, no negative control cells remained, and most tested cell lines yielded no colonies. GFP-positive colonies formed only in Vero cells, and these colonies were expanded for further testing.

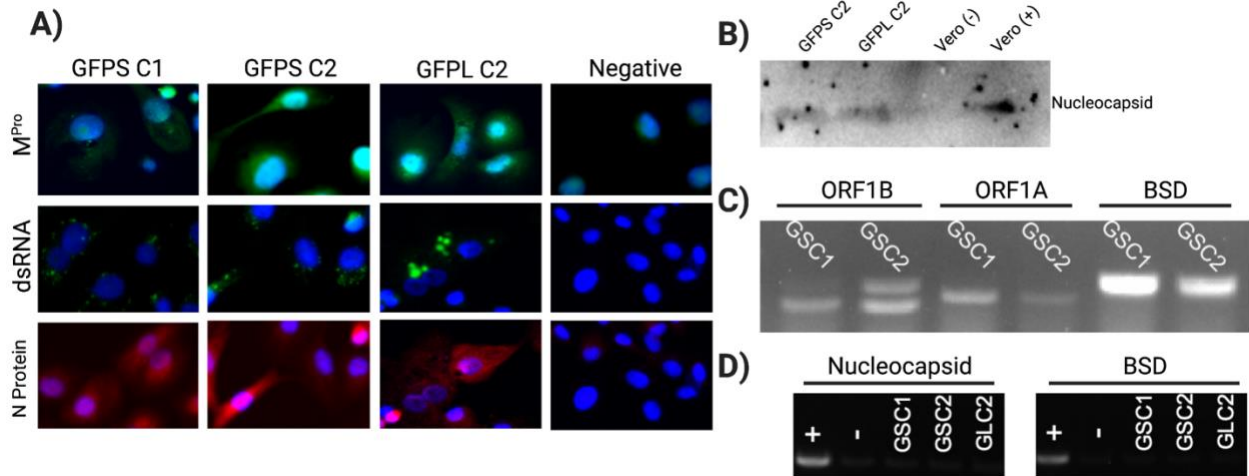


Figure 3.2: Transfected Vero cells show evidence of RNA replication

A) GFP positive Vero cells were stained for the viral proteins nucleocapsid (N) and major protease (M^{Pro}), as well as double stranded RNA (dsRNA), a marker of viral replication. Only GFP-positive cells stained for each antigen. **B)** Both GFPShort and GFPLong designs yield colonies with detectable levels of nucleocapsid protein via Western blot. Untransfected Vero cells served as the negative control, while Vero cells transfected with nucleocapsid RNA served as the positive control. **C)** RNA was extracted from GFP-positive Vero cells and used for RT-PCR. ORF1A, ORF1B and BSD RNAs were detected in multiple clones. **D)** To test if RNA and protein expression were driven by integration of contaminating template DNA, genomic DNA was extracted and used for PCR. None of the tested were positive for integration, suggesting expression is driven by replicon RNA.

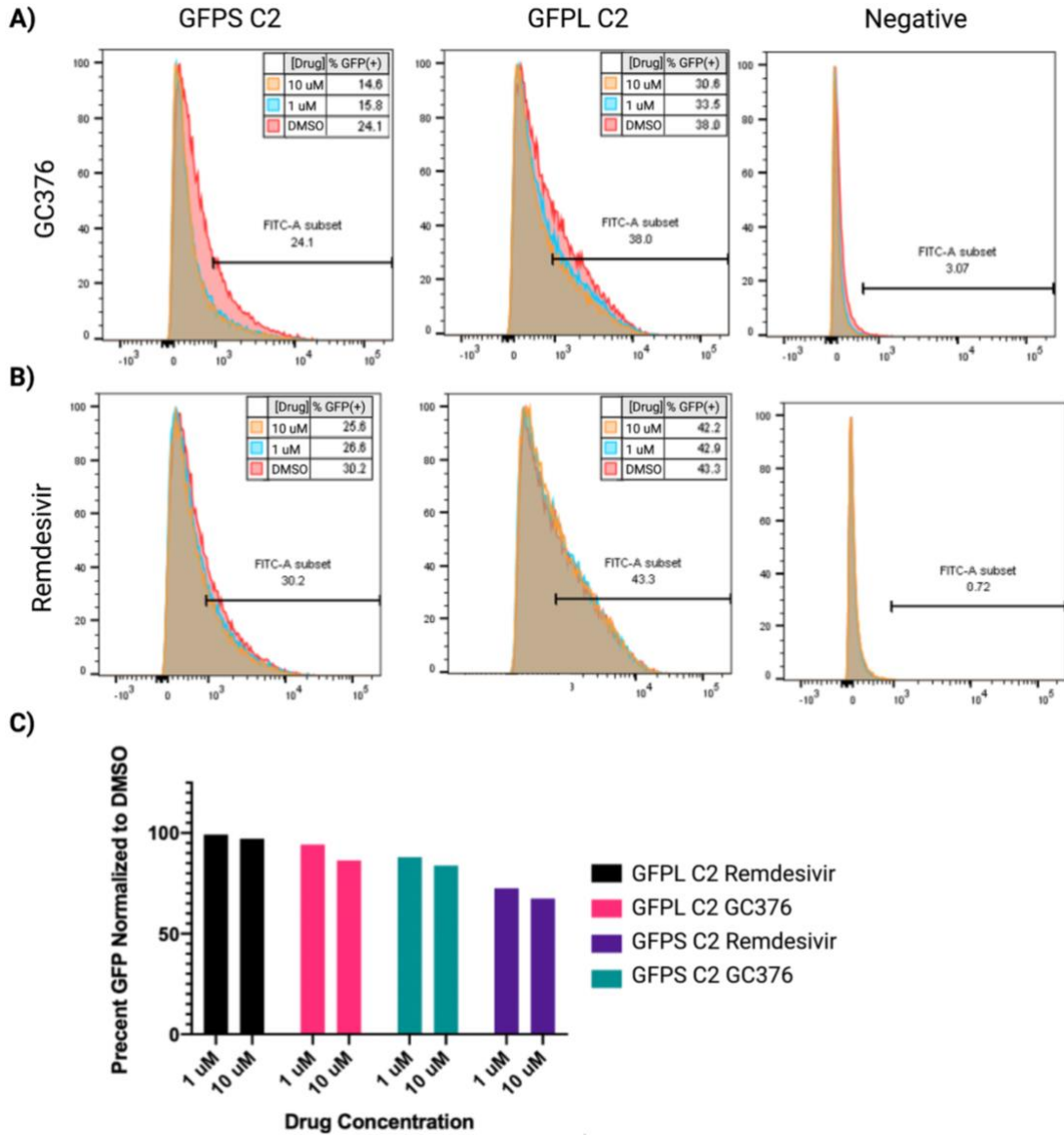


Figure 3.3: Reporter levels in SARS-CoV-2 replicon bearing cells show minimal response to known replication inhibitors.

A) Replicon cells treated with GC376, a major protease (M^{pro}) inhibitor, show a modest reduction in percentage of GFP positive cells in a dose-dependent manner. **B)** Replicon cells treated with remdesivir, an RNA-dependent RNA polymerase inhibitor, show a negligible reduction in percentage of GFP positive cells in a dose-dependent manner. **C)** Graph demonstrating reduction in number of GFP-positive cells normalized to DMSO negative controls.

M TSS Swap



IRES



MPro Site



T2A+IRES



Supplementary Figure 3.1: Alternative replicon designs tested

Additional designs involved introduction of fusion reporter gene into different portions of the viral genome, or replacing the BSD with a zeocin resistance gene (not depicted).

3.7 References

- (1) Wu, F.; Zhao, S.; Yu, B.; Chen, Y.-M.; Wang, W.; Song, Z.-G.; Hu, Y.; Tao, Z.-W.; Tian, J.-H.; Pei, Y.-Y.; Yuan, M.-L.; Zhang, Y.-L.; Dai, F.-H.; Liu, Y.; Wang, Q.-M.; Zheng, J.-J.; Xu, L.; Holmes, E. C.; Zhang, Y.-Z. A New Coronavirus Associated with Human Respiratory Disease in China. *Nature* **2020**, *579* (7798), 265–269.
<https://doi.org/10.1038/s41586-020-2008-3>.
- (2) Almazán, F.; Sola, I.; Zuñiga, S.; Marquez-Jurado, S.; Morales, L.; Becares, M.; Enjuanes, L. Coronavirus Reverse Genetic Systems: Infectious Clones and Replicons. *Virus Research* **2014**, *189*, 262–270. <https://doi.org/10.1016/j.virusres.2014.05.026>.
- (3) Fernandes, R. S.; Freire, M. C. L. C.; Bueno, R. V.; Godoy, A. S.; Gil, L. H. V. G.; Oliva, G. Reporter Replicons for Antiviral Drug Discovery against Positive Single-Stranded RNA Viruses. *Viruses* **2020**, *12* (6), 598. <https://doi.org/10.3390/v12060598>.
- (4) Thiel, V.; Herold, J.; Schelle, B.; Siddell, S. G. Infectious RNA Transcribed in Vitro from a CDNA Copy of the Human Coronavirus Genome Cloned in Vaccinia Virus. *9*.
- (5) Yount, B.; Curtis, K. M.; Fritz, E. A.; Hensley, L. E.; Jahrling, P. B.; Prentice, E.; Denison, M. R.; Geisbert, T. W.; Baric, R. S. Reverse Genetics with a Full-Length Infectious CDNA of Severe Acute Respiratory Syndrome Coronavirus. *Proceedings of the National Academy of Sciences* **2003**, *100* (22), 12995–13000. <https://doi.org/10.1073/pnas.1735582100>.
- (6) Ge, F.; Luo, Y.; Liew, P. X.; Hung, E. Derivation of a Novel SARS–Coronavirus Replicon Cell Line and Its Application for Anti-SARS Drug Screening. *Virology* **2007**, *360* (1), 150–158. <https://doi.org/10.1016/j.virol.2006.10.016>.
- (7) Xie, X.; Muruato, A. E.; Zhang, X.; Lokugamage, K. G.; Fontes-Garfias, C. R.; Zou, J.; Liu, J.; Ren, P.; Balakrishnan, M.; Cihlar, T.; Tseng, C.-T. K.; Makino, S.; Menachery, V. D.;

- Bilello, J. P.; Shi, P.-Y. *A Nanoluciferase SARS-CoV-2 for Rapid Neutralization Testing and Screening of Anti-Infective Drugs for COVID-19*; preprint; Microbiology, 2020.
<https://doi.org/10.1101/2020.06.22.165712>.
- (8) Xie, X.; Muruato, A.; Lokugamage, K. G.; Narayanan, K.; Zhang, X.; Zou, J.; Liu, J.; Schindewolf, C.; Bopp, N. E.; Aguilar, P. V.; Plante, K. S.; Weaver, S. C.; Makino, S.; LeDuc, J. W.; Menachery, V. D.; Shi, P.-Y. An Infectious CDNA Clone of SARS-CoV-2. *Cell Host & Microbe* **2020**, S1931312820302316.
<https://doi.org/10.1016/j.chom.2020.04.004>.
- (9) Thi Nhu Thao, T.; Labroussaa, F.; Ebert, N.; V'kovski, P.; Stalder, H.; Portmann, J.; Kelly, J.; Steiner, S.; Holwerda, M.; Kratzel, A.; Gultom, M.; Schmied, K.; Laloli, L.; Hüsser, L.; Wider, M.; Pfaender, S.; Hirt, D.; Cippà, V.; Crespo-Pomar, S.; Schröder, S.; Muth, D.; Niemeyer, D.; Corman, V. M.; Müller, M. A.; Drosten, C.; Dijkman, R.; Jores, J.; Thiel, V. Rapid Reconstruction of SARS-CoV-2 Using a Synthetic Genomics Platform. *Nature* **2020**, 582 (7813), 561–565. <https://doi.org/10.1038/s41586-020-2294-9>.
- (10) Lan, S.; Tedbury, P. R.; Ong, Y. T.; Shah, R.; Slack, R. L.; Cilento, M. E.; Zhang, H.; Du, H.; Lulkin, N.; Le, U. Q.; Kirby, K. A.; Melcak, I.; Cantara, W. A.; Boggs, E. A.; Sarafianos, S. G. *Subgenomic SARS-CoV-2 Replicon and Reporter Replicon Cell Lines Enable Ultrahigh Throughput Antiviral Screening and Mechanistic Studies with Antivirals, Viral Mutations or Host Factors That Affect COVID-19 Replication*; preprint; Microbiology, 2021. <https://doi.org/10.1101/2021.12.29.474471>.
- (11) Ricardo-Lax, I.; Luna, J. M.; Thao, T. T. N.; Le Pen, J.; Yu, Y.; Hoffmann, H.-H.; Schneider, W. M.; Razooky, B. S.; Fernandez-Martinez, J.; Schmidt, F.; Weisblum, Y.; Trüeb, B. S.; Berenguer Veiga, I.; Schmied, K.; Ebert, N.; Michailidis, E.; Peace, A.;

- Sánchez-Rivera, F. J.; Lowe, S. W.; Rout, M. P.; Hatziioannou, T.; Bieniasz, P. D.; Poirier, J. T.; MacDonald, M. R.; Thiel, V.; Rice, C. M. Replication and Single-Cycle Delivery of SARS-CoV-2 Replicons. *Science* **2021**, *374* (6571), 1099–1106.
<https://doi.org/10.1126/science.abj8430>.
- (12) Kotaki, T.; Xie, X.; Shi, P.-Y.; Kameoka, M. A PCR Amplicon-Based SARS-CoV-2 Replicon for Antiviral Evaluation. *Sci Rep* **2021**, *11* (1), 2229.
<https://doi.org/10.1038/s41598-021-82055-0>.
- (13) Nguyen, H. T.; Falzarano, D.; Gerdts, V.; Liu, Q. Construction of a Noninfectious SARS-CoV-2 Replicon for Antiviral-Drug Testing and Gene Function Studies. *J Virol* **2021**, *95* (18), e00687-21. <https://doi.org/10.1128/JVI.00687-21>.
- (14) Liu, S.; Chou, C.-K.; Wu, W. W.; Luan, B.; Wang, T. T. *Stable Cell Clones Harboring Self-Replicating SARS-CoV-2 RNAs for Drug Screen*; preprint; Microbiology, 2021.
<https://doi.org/10.1101/2021.11.04.467291>.
- (15) Savastano, A.; Ibáñez de Opakua, A.; Rankovic, M.; Zweckstetter, M. Nucleocapsid Protein of SARS-CoV-2 Phase Separates into RNA-Rich Polymerase-Containing Condensates. *Nat Commun* **2020**, *11* (1), 6041. <https://doi.org/10.1038/s41467-020-19843-1>.

Concluding remarks

We sought to demonstrate the effects CHIP's Hsp-independent enzymatic activity has in cellular contexts in a bid to elucidate molecular underpinnings of multiple disease states, including neurodegeneration, cancer, and viral infections. Towards this goal, we were successful in generating potent and novel inhibitors of CHIP (chapter 1) and provide some preliminary insights into Hsp-independent CHIP functions in HHV-8 (chapter 2), despite a global pandemic interrupting these efforts and redirecting research towards developing viral replicons (chapter 3). While these results are exciting, there remain many unanswered questions.

While we thoroughly characterized the Fabs from chapter 1, there are multiple unanswered questions that can be addressed. First, it is unknown if CHIP's role in some disease states is binding mediated or ubiquitination mediated. Future studies can use Fab 2D11 to examine the role of ubiquitination independent of substrate binding. Second, with additional interest in the dimer-monomer equilibrium of CHIP, examination of the effects of these antibodies in cells on autoubiquitination and the dimer-monomer equilibrium in cells could be of interest. Next, since 2C5 does not impact any assessed CHIP function, but has reasonable affinity for CHIP, it would be interesting to use it as a PROTAC effector. Finally, after these antibodies undergo additional mechanism testing, their *in vivo* inhibition of CHIP could enable resolution of CHIP's role in proteostasis in a time and cell dependent manner.

Next, the predicted, Hsp-independent, CHIP interaction with the HHV-8 protein ORF28 seems to be a true interaction, and some preliminary data indicates the interaction may alter host protein levels. However, the host proteins affected by the interaction were identified using proteomic approaches and have not been independently verified. Additionally, further studies would benefit from using a cell line more relevant to HHV-8 replication, as the current proteomics work was done in HEK293 cells. While the preliminary data generated focused on the idea the primary function of this interaction is to mediate ubiquitination of host proteins to improve viral fitness, this interaction may also serve as a mechanism of CHIP inhibition to free additional Hsp for folding viral proteins during replication.

Publishing Agreement

It is the policy of the University to encourage open access and broad distribution of all theses, dissertations, and manuscripts. The Graduate Division will facilitate the distribution of UCSF theses, dissertations, and manuscripts to the UCSF Library for open access and distribution. UCSF will make such theses, dissertations, and manuscripts accessible to the public and will take reasonable steps to preserve these works in perpetuity.

I hereby grant the non-exclusive, perpetual right to The Regents of the University of California to reproduce, publicly display, distribute, preserve, and publish copies of my thesis, dissertation, or manuscript in any form or media, now existing or later derived, including access online for teaching, research, and public service purposes.

DocuSigned by:

Emily Connelly

70DC7AF28EE7410...

Author Signature

5/18/2023

Date